Universität Zürich
Zentrum für Zahnmedizin
Klinik für Kaufunktionsstörungen, abnehmbare Rekonstruktionen,
Alters- und Behindertenzahnmedizin
Direktor: Prof. Dr. sc. techn. Luigi M. Gallo

Arbeit unter Leitung von
PD Dr. med. et med. dent. Dominik A. Ettlin
und Prof. Dr. sc. techn. Luigi M. Gallo

3D-reconstruction and evaluation of MR images of children with juvenile idiopathic arthritis (JIA)

INAUGURAL-DISSERTATION
zur Erlangung der Doktorwürde der Zahnmedizin
der Medizinischen Fakultät
der Universität Zürich

vorgelegt von
Mei-Yin Hou
von Greifensee ZH

Genehmigt auf Antrag von Prof. Dr. sc. techn. Luigi M. Gallo
Zürich 2012

Table of Contents

1 Abstract 3
2 Zusammenfassung 5
3 Introduction 7
4 Aim of the study 10
5 Materials and methods 11
5.1 Subjects 11
5.2 TMJ magnetic resonance imaging 11
5.3 3D-reconstructions and quantitative measurements 12
5.4 Statistical analysis 16
6 Results 18
6.1 Subjects characteristics 18
6.2 Description of TMJ morphology 18
6.2.1 Intercondylar angle 18
6.2.2 Condylar volume 19
6.2.3 Anterior fossa slope (steepness and length) 19
6.2.4 Medio-lateral and antero-posterior diameters of the condyle 20
6.3 Intra- and interindividual comparisons 21
7 Discussion 24
8 Conclusion 28
9 Tables 29
10 Figures 40
11 References 61
12 Acknowledgements 64
13 Appendix A 65
14 Curriculum Vitae 75

1 Abstract

Objectives. 1) Virtual bilateral TMJ reconstruction from magnetic resonance (MR) imaging of 28 children (age range: 2.7 - 16.9) with juvenile idiopathic arthritis (JIA) by means of state-of-the-art software and 2) quantitative intra- and interindividual comparison of joint deformation.

Methods. MR sections of all joints were assessed by two pediatric radiologists and reconstructed using Amira™. Subjects were divided into three age groups and two diagnostic groups (no/mild vs. severe deformation). After ascertaining normal distribution, intra- and interindividual joint comparisons were performed with ANOVA and t-tests at $\alpha=0.05$. Parameters not differing between sides and/or plane orientation were averaged intra-individually.

Results. Significant differences among age groups were found for: steepness of the anterior fossa slope ($p=0.003$), condylar volume ($p=0.007$), intercondylar angle ($p=0.008$), direct and curvilinear length of the anterior fossa slope ($p=0.047$ resp. 0.009) and medio-lateral condylar diameter (left $p=0.023$, right $p=0.017$). Severely deformed TMJs had a smaller intercondylar angle ($p=0.009$) and a shallower anterior fossa slope ($p=0.021$) than normal or mildly deformed joints.

Conclusion. Virtual 3D-reconstruction of TMJs of JIA children is feasible without ionizing radiation, but requires time and special skills. Across age groups and independent of radiological disease evidence, measurements on virtual models reflected morphological changes observed with conventional radiography during growth. Due to limited patient numbers in each age group, diagnostic (sub)groups could only be formed across all subjects. 3D-parameters of severely deformed joints seem to reflect altered joint growth and development. Future studies with larger cohorts may reveal further differences and should include healthy controls.

2 Zusammenfassung

Hintergrund. Die juvenile idiopathische Arthritis (JIA) ist die häufigste rheumatische Erkrankung in der Kindheit. Die Prävalenz liegt zwischen 0.07 - 4.01 pro 1000 Kindern, wobei Mädchen dreimal häufiger erkranken. JIA tritt meistens zwischen dem 2. - 4., resp. dem 8. - 10. Lebensjahr auf. Je nach Untersuchungsmethode und Studienpopulation ist das Kiefergelenk in 17 - 87 % der Patienten befallen und kann sowohl das initiale, wie auch das einzig betroffene Gelenk sein. Der Verlauf der Krankheit variiert individuell stark. Mögliche Komplikationen beinhalten Schwellung und Steifheit des Gelenks, Mundöffnungsschwierigkeiten und Schmerzen beim Kauen und Entwicklungsstörungen des Kauapparates resultierend in funktioneller wie auch morphologischer Beeinträchtigung. Eine möglichst frühe Diagnose und Therapie ist deshalb von essentieller Bedeutung.
Der heutige Goldstandard zur Detektion von Kiefergelenksbefall mittels Bildgebung ist die Magnetresonanztomographie (MRT). Bisherige Studien haben hauptsächlich zweidimensionale Charakteristika von JIA Patienten gezeigt. Neue Technologien sind heutzutage verfügbar, um eine dreidimensionale Darstellung, sowie Analyse und Quantifizierung der rekonstruierten Modelle zu ermöglichen.

Ziele. Virtuelle Rekonstruktion von 56 Kiefergelenken aus Magnetresonanzaufnahmen von 28 Kindern mit JIA und Quantifizierung, sowie Analyse der rekonstruierten Modelle mittels verschiedener morphologischer Parameter inter- und intraindividuell.

Methoden. MRT von allen Gelenken wurden vorgängig von zwei Kinderradiologen beurteilt und dann mittels Amira™ rekonstruiert. Es wurden drei Altersgruppen und zwei diagnostische Gruppen (keine/milde Deformation vs. schwere Deformation) gebildet. Normalverteilung wurde ermittelt und intra- und interindividuelle Vergleiche wurden mit ANOVA und t-test bei $\alpha=0.05$ ausgeführt. Parameter, welche keine intraindividuellen Seitenunterschiede und/oder Unterschiede der Schnittebenen gezeigt haben, wurden für die weitere Datenanalyse gemittelt.

Resultate. Signifikante Unterschiede in den drei Altersgruppen wurden für folgene Parameter gefunden: Steilheit der Steigung der anterioren Fossa ($p=0.003$), Kondylenvolumen ($p=0.007$), interkondylärer Winkel ($p=0.008$), direkte und effektive Länge der Steigung der anterioren Fossa ($p=0.047$ resp. 0.009) und medio-lateraler Diameter des Kondylus (links $p=0.023$, rechts $p=0.017$). Schwer deformierte Kiefergelenke zeigten einen kleineren interkondylären Winkel ($p=0.009$) und eine flachere anteriore Fossa ($p=0.021$).

Schlussfolgerung. Virtuelle 3D-Rekonstruktion von Kiefergelenken ist ohne ionisierende Strahlung möglich. Über die Altersgruppen und unabhängig vom radiologischen Befund zeigten die Messungen morphologische Veränderungen entsprechend der bei konventioneller Radiographie beobachteten Wachstumsentwicklung. Schwer deformierte Gelenke scheinen eine veränderte Wachstumsentwicklung vorzuweisen. Zukünftige Studien mit grösseren Kohorten könnten weitere Unterschiede aufzeigen und sollten gesunde Kontrollen beinhalten.

3 Introduction

Juvenile idiopathic arthritis (JIA) is the most frequent rheumatic disease in childhood (Gare, 1996). Diagnostic criteria for JIA include

a) onset of disease before the age of 16,

b) duration of arthritis longer than six weeks, and

c) exclusion of so far identifiable causes (including trauma and bacterial infections).

JIA was first described by Still in 1897. Its prevalence was reported to lie between 0.07 and 4.01 per 1000 individuals and the annual incidence between 0.01 and 0.23 per 1000 individuals. Females are three times more likely to be affected than males (Farronato et al., 2010). The disease outbreak occurs most commonly between the age of two and four years and then again between eight and ten years (Karhulahti et al., 1993). Progression of the disease varies individually, and, as a result, an accurate prediction of the progression is difficult. Worse outcome has been reported especially for patients with systemic or polyarticular arthritis, patients at a young age of disease onset, female patients, and patients with an extended disease course. Serious complications of the disease include joint swelling and stiffness, uveitis (possibly leading to blindness), and growth disturbances. The objectives of therapy are full remission of JIA, prevention of growth disturbances and preservation of everyday functions.

In JIA, the temporomandibular joint (TMJ) is affected in 17 – 87 % of cases, depending on examination methods applied and population studied (Mayne and Hatch, 1969; Ronning et al., 1974; Kuseler et al., 1998). In 30 – 50% of cases, unilateral involvement was reported.

Incidence varies widely based upon subtype of JIA: it has been reported that patients with antinuclear antibodies (ANA) have a higher prevalence of condylar resorption. In contrast, those with a positive human leukocyte antigen B27 (HLA-B27) titer have a lower risk of TMJ involvement (Karhulahti et al., 1993; Hu et al., 1996; Twilt et al., 2004). Of particular importance is the fact that the TMJ may be the initial and even the only joint affected (Martini et al., 2001; Scolozzi et al., 2005). TMJ involvement can result in abnormalities including micrognathia (30%) and malocclusion (69%) (Karhulahti et al., 1993; Pedersen et al., 2001). Other possible complications include decreased and/or asymmetric mouth opening, chewing difficulties and pain upon jaw movement. This can lead to adopting a jaw posture to minimize pain, which may lead to muscle atrophy. Thus, early diagnosis of JIA affecting the TMJ is of special concern to prevent irreversible growth disorders resulting in mandibular dysfunction and dysmorphic facial features.

Early detection of TMJ arthritis is a diagnostic challenge, as patients often present no clear clinical signs and symptoms, and symptoms frequently fluctuate. Currently, the gold standard for screening TMJ involvement is magnetic resonance imaging (MRI). Other methods, such as ultrasound and rheumatologic/orthodontic examination are less sensitive/specific than MRI (Müller et al., 2009). These facts often lead to diagnostic delays, thus resulting in undetected progression of inflammation and possible damage of the growing joint and thus hampered mandibular development. By the time asymmetry or retrognathism becomes evident, irreversible damage to the condylar growth zone has already occurred. Therefore, again, it is of utmost importance to detect and treat TMJ involvement as early as possible.

Previous imaging studies mostly using conventional planar projections (lateral, postero-anterior, transcranial and panoramic radiographs), computer tomography, MRI, echography, or radionuclide bone scans have to date only shown two-dimensional (2D) TMJ characteristics of JIA patients. New technologies nowadays are available to assess TMJ morphology three-dimensionally (3D) by constructing virtual software models of the joints that yield interactive visualization and enable morphology quantification. Namely, the use of CBCT (cone beam computerized tomography) and MRI have opened a new perspective on visualization and diagnosis of osseous structures. Condylar resorption areas overseen under 2D analysis may be unveiled and otherwise undetected morphologic variations may be newly discovered (Costa et al., 2008; Cevidanes et al., 2010). In JIA, only few research groups have so far reported on MRI-based TMJ 3D-reconstructions (Kitai et al., 2002). Several studies have proposed new methods to reconstruct and analyze 3D TMJ using CBCT and will be discussed later (Cevidanes et al., 2010; Farronato et al., 2010). Owing to the lack of ionizing radiation exposure, TMJ 3D-assessment based on MRI may ultimately provide a repeatable objective method - quantitative as well as volumetric - for monitoring the course of disease in young subjects and the effects of intervention from an early age on.

4 Aim of the study

The objectives of this study were

1) to virtually reconstruct from MRI recordings both TMJs of 28 JIA children, *i.e.* 56 joints, by using a state-of-the-art image processing software for interactive visualization,
   and
2) to quantitatively assess and compare joint deformation within and between subjects by performing morphological measurements of the 3D-reconstructions.

5 Materials and methods

5.1 Subjects

MRI data was obtained from 28 children (15 female, 13 male) with a mean age of 9.1 years (range 2.7 – 16.9). All children were diagnosed according to the International League of Associations for Rheumatology (ILAR) criteria of Edmonton (2001) (Petty et al., 2001) and included in the study after informed consent was obtained. Exclusion criteria consisted of a previous diagnosis of TMJ arthritis and/or performance of MRI of the TMJ within the past 6 months and/or orthodontic treatment within the past 12 months. Approval by the Institutional and Governmental Ethics Review Board had been given (data collection was part of the study by *Müller et al., 2009*). For detailed subject characteristics please refer to chapter 9, Table 1.

5.2 TMJ magnetic resonance imaging

MRIs were recorded on a 1.5 T scanner (Signa MR/i Twinspeed HDx, GE Medical Systems, Milwaukee, WI, USA) at the Pediatric Hospital, University of Zurich, Switzerland. Examinations were performed with a dedicated TMJ coil in closed mouth position separately for each TMJ with oblique sagittal 3D gradient-echo sequences (TR/TE/flip angle, 12ms/3.9ms/20°). Imaging parameters consisted of 2 mm slice thickness with a 1 mm interslice gap, with a total of 20 – 24 slices from lateral to medial. Images were made with a 256 × 192 matrix and a 100 cm field of view.

All MR images were assessed by two pediatric radiologists and diagnostic decisions were reached by consensus. Outcome variables

evaluated were a) excess joint fluid, b) increased contrast enhancement and c) condylar deformity (for further information see *Müller et al., 2009*):

- The amount of joint fluid in T2-weighted images was considered normal when small dots or lines of high signal were visible in a joint recess without distensions.
- Joint enhancement in fat-saturated T1-weighted images was considered normal when high signal confined to IA fluid was visible as delineated on the T2-weighted images. Abnormal joint enhancement was graded as increased or prominent: for *increased enhancement* the signal of the synovial membrane had to be hyperintense to muscle, for *prominent enhancement* the synovial membrane had to be thickened and the signal isointense to vessels. Increased joint fluid and/or increased enhancement were considered indicative of active inflammation.
- Condylar deformity was graded as mild or severe: *mild deformity* was diagnosed when only the anterior or posterior circumference was flattened and *severe deformity* when the condyle was squared with loss of height.

Disc position and disc morphology were not evaluated, since studies have shown that these features vary widely among healthy children and adults (Smith et al., 1992; Kuseler et al., 1998) and disc position is often normal in joints with chronic arthritic disease involvement (Larheim et al., 1992).

5.3 3D-reconstructions and quantitative measurements

Segmentation in the sagittal plane was performed by outlining the structures visible on the MRI slices with a pen tablet (Intuos3 9×12,

Wacom, Japan). The contours of the mandibular condyle and glenoid fossa were thus obtained for each subject. 3D-reconstruction of these structures was carried out by using the software Amira™ (Visage Imaging Inc., San Diego, CA, USA). Interpolation and smoothing was utilized to improve surface quality within the limits of the original morphology.

For images of all reconstructed joints cfr. Appendix A.

For each subject, following parameters (in italics) were determined in either Amira™ or Rhinoceros 4.0™ (McNeel, Seattle, WA, USA):

- The *intercondylar angle* (*i.e.* the angle between both condylar axes) was measured between both main intracondylar axes running through the condylar poles (Fig. 5.3.1).

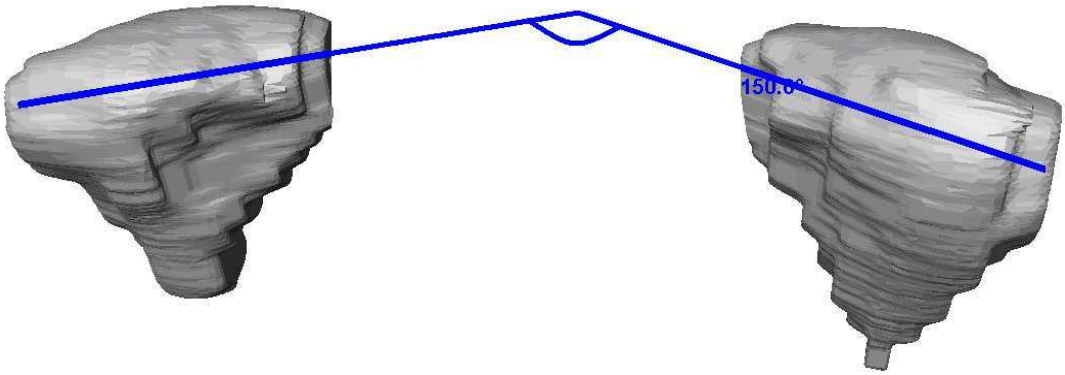

Figure 5.3.1. Determination of the intercondylar angle (Amira™ software).

- The *condylar volume* was obtained after exporting the TMJ model files into Rhinoceros 4.0™. For condylar volume computations, condylar heads and condylar necks needed to be delineated by the following registration procedure: first, transversal axes of both condyles were automatically aligned perpendicularly to the sagittal plane. Subsequently, visible surfaces were superimposed until maximum alignment of the condylar necks was reached. Finally, both condylar models were cut at the same level and separated from the proximal necks (Fig. 5.3.2).

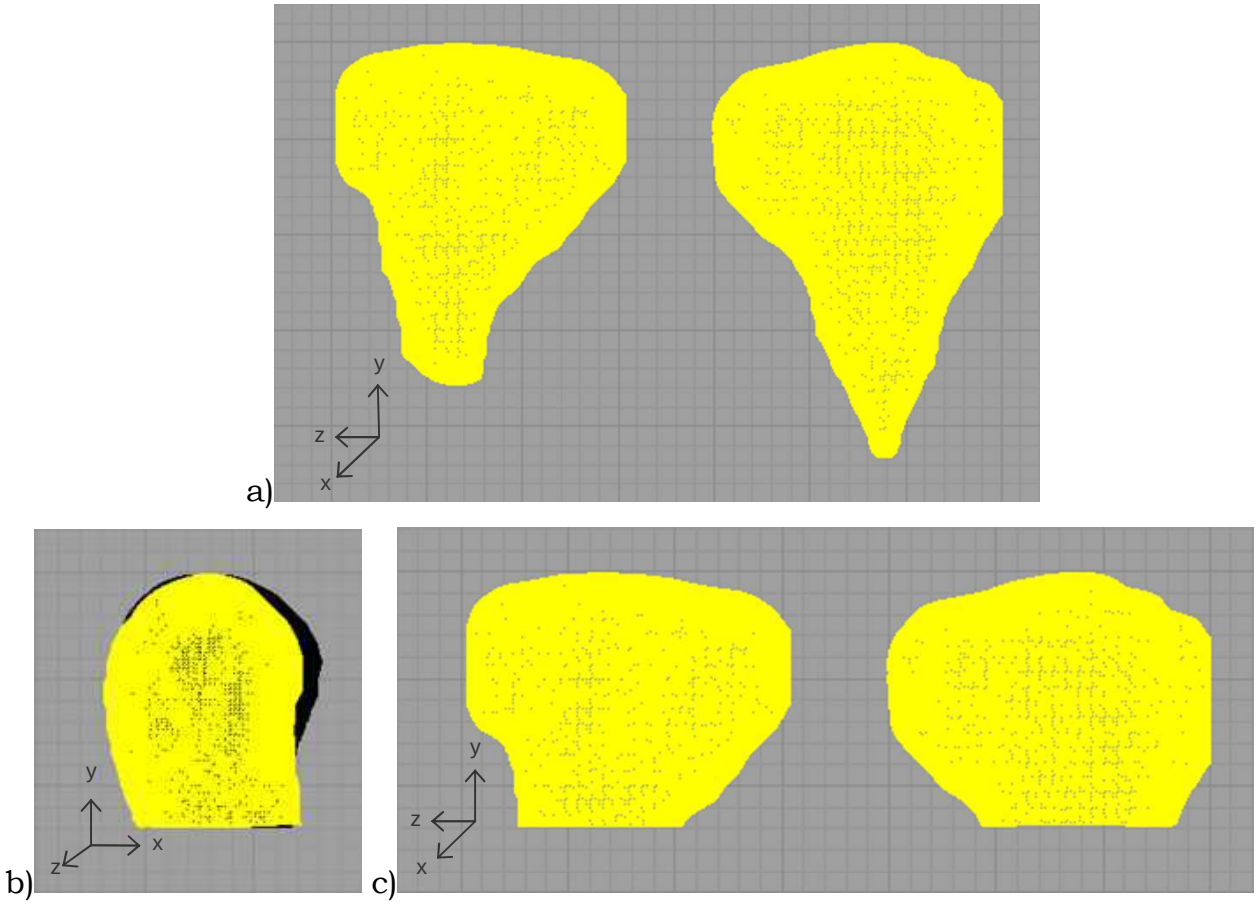

Figure 5.3.2. Procedure for determining the condylar volumes. a) Condylar model files segmented in Amira™ were exported to Rhinoceros4.0™ (frontal view). b) The surfaces were superimposed, aligned at the apex, and then truncated caudally at the same level at the condylar neck (sagittal view). c) The condylar images were then re-separated (frontal view).

- The *steepness of the anterior fossa slope* was measured by connecting its highest and lowest points on a parasagittal median section (*i.e.* perpendicular to the main condylar axis). Thereafter, we determined the angle formed by this linear segment with the horizontal plane. Additionally, this parameter was calculated on a sagittal section. Figure 5.3.3 shows the determination of the *steepness of the anterior fossa slope* in the parasagittal median section (marked in pink).

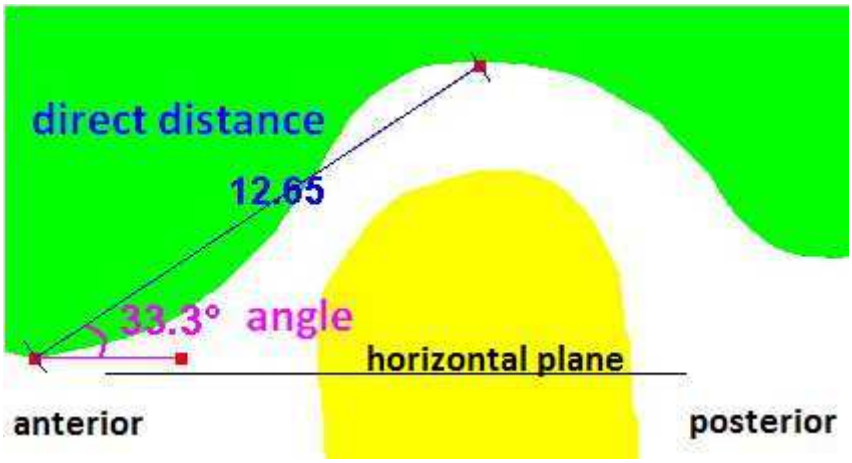

Figure 5.3.3. Measurement of steepness and length of the anterior fossa slope (Amira™ software).

- The *direct length of the anterior fossa slope* was determined by measuring the distance between its cranial and caudal horizontal tangent points on a parasagittal median section (*i.e.* perpendicular to the main condylar axis). Figure 5.3.3 shows the determination of the direct length of the anterior fossa slope in the parasagittal median section (marked in blue).
- The *curvilinear length of the anterior fossa slope* was determined along the fossa contour between the two tangential points mentioned above. Figure 5.3.4 shows the procedure.

  Both length parameters of the fossa were also calculated on a sagittal section.

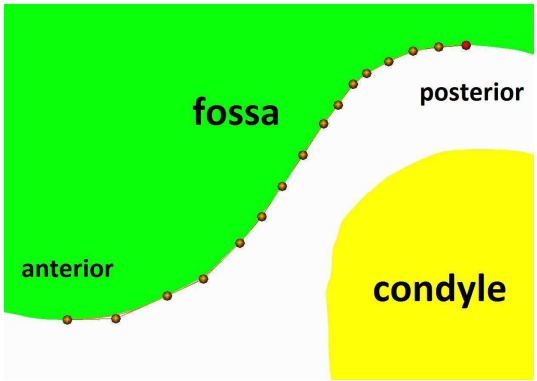

Figure 5.3.4. Measurement of the curvilinear length (Amira™ software).

- For each condyle, the largest transversal section was selected and the *medio-lateral* and the *antero-posterior diameters* were measured (Fig. 5.3.5; top view).

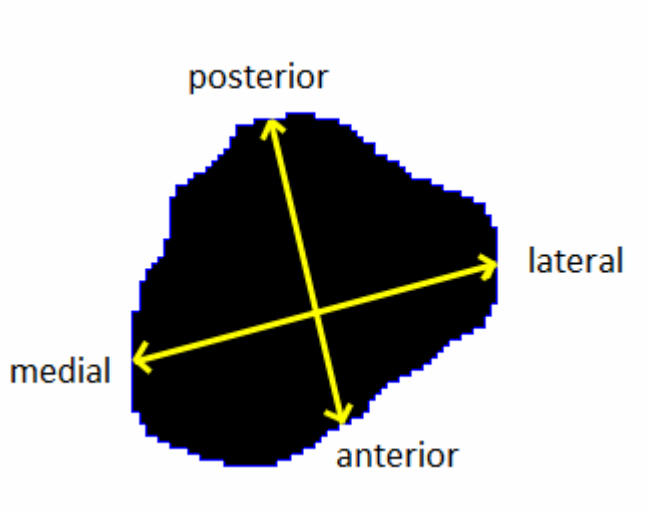

Figure 5.3.5. Measurement of medio-lateral and antero-posterior diameter of the condyle on the largest transversal section (Amira™ software).

5.4 Statistical analysis

Data were analyzed by means of descriptive statistical parameters (mean, standard deviation, median, minimum and maximum). Data were also presented in box plots and analyzed for normality according to Kolmogorov-Smirnov and Shapiro-Wilk tests. Intraindividual differences between sides and between orientation (sagittal and parasagittal) were analyzed by paired t-tests or ANOVA for repeated measurements if the data was normally distributed. For data reduction, parameters were averaged between sides or between sagittal and parasagittal orientation when no statistically significant differences were found. For non-normally distributed data, interindividual differences were assessed by means of Mann-Whitney U- or Kruskal-Wallis tests. Significance level was set at $\alpha=0.05$, $p\geq0.05$ being non-significant (n.s.). For $0.01\leq p<0.05$ differences were

considered significant (denoted by one asterisk *), for $0.001 \leq p < 0.01$ differences were considered highly significant (denoted by two asterisks **), and for $p < 0.001$ differences were considered extremely significant (denoted by three asterisks ***). All statistical analyses were performed by means of SPSS™ for Windows Version 18.

6 Results

6.1 Subjects characteristics

Table 9.1 shows the demographic data of the subjects analyzed. The 28 children (15 female, 13 male) presented with a median age of 9.1 years (range 2.7 – 16.9). Median height was 138.0 cm (range 96.3 – 166.3) and median weight 29.4 kg (range 14.6 – 61.0). Median disease duration was 2.5 years (range 0.1 – 12.2), based on the date of first diagnosis reported in medical records. Ten children had oligoarthritis, 3 had extended oligoarthritis, 11 had polyarthritis, one had psoriatic arthritis and 3 had enthesitis related arthritis. All children were rheumatoid factor (RF) negative. Nineteen children were antinuclear antibodies (ANA) positive. One child had a positive HLA-B27 titer; three had missing data, and all others were HLA-B27 negative. Four children were diagnosed with uveitis.

6.2 Description of TMJ morphology

6.2.1 Intercondylar angle

Values of the intercondylar angles (see section 5.3) are listed in Table 9.2 and summarized in the box plot of Figure 10.1. They ranged between 119.7° (subject no. 28) and 158.0° (subject no. 11), median angle was 140.4°.

6.2.2 Condylar volume

Condylar volumes were computed as described in section 5.3. for each condyle. The ratio was calculated by dividing the greater volume by the smaller one.

Table 9.3 lists the values of the condylar volumes and their ratio for each subject. These values are summarized in the box plots of Figures 10.2 and 10.3. Overall volumes ranged widely from 329 mm^3 (subject no. 26) to 1382 mm^3 (subject no. 3), median volume was 697.5 mm^3 (range 329.0 – 1382.0) for the right condyles, respectively 719.5 mm^3 (range 376.0 – 1106.0) for the left.

Left condyles were larger in 16 subjects and right condyles in 9 subjects; in three subjects left and right volumes were almost equal (subjects no. 10, 15 and 18: ratio <1.05). Median ratio for all subjects was 1.15 (range 1.01 – 1.45), 1.0 meaning both condyles had the same volume.

6.2.3 Anterior fossa slope (steepness and length)

Table 9.4 lists the values of the *steepness* of the anterior fossa slope for all joints. These values are summarized in Figure 10.4.

The steepness of the anterior fossa slope ranged overall between 2.5° and 49.7°, median angles were 31.6° (range 14.3 – 46.5) for the right, respectively 31.3° (range 12.9 – 49.7) for the left side in the parasagittal median section and 30.6° (range 2.5 – 42.3) for the right, respectively 31.5° (range 8.9 – 47.2) for the left side in the sagittal section.

Among all subjects, steepest fossa measurements were found bilaterally in subject no. 9 in both sagittal and parasagittal

orientation; shallowest fossae were observed in two subjects (no. 18 and 25).

Table 9.5 lists the values of the *direct length* of the anterior fossa slope for all joints. These values are summarized in Figure 10.5.
The direct length of the anterior fossa slope ranged from 3.9 mm to 16.4 mm. The smallest lengths for both orientations were found in subject no. 25. The greatest length in the parasagittal median section was found in subject no. 17. The greatest length in the sagittal median section was found in subject no. 8.

The values of the *curvilinear length* of the anterior fossa slope are reported in Table 9.6 for all joints and their distribution is shown in Figure 10.6.
The curvilinear length of the anterior fossa slope ranged from 4.8 mm to 17.3 mm. The smallest lengths for both sections were found in the same subject as for the smallest direct lengths (subject no. 25). The greatest curvilinear lengths were found in subject 2 (sagittal section) and 17 (parasagittal section).

6.2.4 Medio-lateral and antero-posterior diameters of the condyle

The values of the medio-lateral and antero-posterior diameters for all condyles are listed in Table 9.7 and summarized in Figure 10.7.
The *medio-lateral* diameter ranged from 10.4 mm (subject no. 6) to 18.4 mm (subject no. 23), the median value being 15.6 mm (range 10.7 – 18.4) for the right, respectively 15.4 mm (range 10.4 – 17.5) for the left condyle.

The *antero-posterior* diameter ranged from 5.1 mm to 11.8 mm, median value being 7.7 (range 5.9 – 11.1) for the right, respectively 7.7 (range 5.1 – 11.8) for the left condyle. The largest diameters for the left and right condyle were found in subject no. 6 and the smallest diameters in subject no. 14.

6.3 Intra- and interindividual comparisons

Subjects were divided in three age categories: first group (0 – 6 years, 6 subjects), second group (6 – 12 years, 18 subjects) and third group (12 – 18 years, 4 subjects).

All 56 joints were graded by two expert pediatric radiologists who assessed the MR images based on three variables: joint fluid, contrast enhancement and joint deformity. Detailed results can be found in Table 9.8. Condylar images were divided into two diagnostic groups, one group with the joints graded as no or mild joint deformation (group A), the other with the joints graded as severe deformation (group B) (Table 9.9 and Table 9.10). Subjects no. 21 and 23 were graded with unilateral deformation of the left condyle.

The reconstructed joints scored as “severe deformation” are shown in Figures 10.8 – 10.14. All seven subjects grouped as severely deformed were diagnosed either with polyarthritis (4 subjects), oligoarthritis (one subject) or extended oligoarthritis (2 subjects). All of them were tested antinuclear antibodies (ANA) positive, had no rheumatoid factor (RF), and were HLA-B27 negative (except one unknown). Two subjects were diagnosed with uveitis.

All unilateral parameters were inter-individually normally distributed according to Kolmogorov-Smirnov and Shapiro-Wilk tests. Following

parameters were averaged intra-individually since they did not differ between the sides and/or between the sagittal and parasagittal orientation: condylar volume (averaged left and right, p = 0.420), steepness of the anterior fossa slope (averaged left and right, p = 0.919) for sagittal and parasagittal section, direct length (averaged left and right, and sagittally and parasagittally, p = 0.415 resp. p = 0.420), and curvilinear length (averaged left and right, and sagittally and parasagittally, p = 0.852 resp. p = 0.100). All other parameters remained original and a new data set was generated.

Results of the comparison of the parameters across the three age categories (*0 – 6 years, 6 – 12 years, 12 – 18 years*) are shown in Table 9.11. Box plots are shown in Fig. 10.15 – 10.25. Significant differences among the three age groups were found for age at diagnosis (p = 0.025), direct length of the anterior fossa slope (p = 0.047) and medio-lateral diameters (left p = 0.023 and right p = 0.017). Weight (p = 0.001), intercondylar angle (p = 0.008), condylar volume (p = 0.007), steepness of the anterior fossa slope in the parasagittal and sagittal orientation (both p = 0.003) and curvilinear length (p = 0.009) differed highly significantly among the age groups. Finally, height differed extremely significant (p < 0.001). Bonferroni post-hoc tests (Table 9.12) showed no significant difference between group 2 and 3 for age at diagnosis, intercondylar angle, condylar volume, steepness of the anterior fossa slope, fossa lengths and medio-lateral diameter. Condylar volume did not differ significantly also between group 1 and 2.

Figures 10.26 – 10.38 show the box plots of the comparisons of group A (*no or mild joint deformation*) with group B (*severe joint deformation*). Results of the comparison between these two diagnostic groups are shown in Table 9.13. The differences of the intercondylar angles as

well as of the antero-posterior diameters of the right condyles were highly significant (p = 0.009 resp. p = 0.003). The steepness of the anterior fossa slope differed significantly between the two groups in the parasagittal as well as in the sagittal orientation (p = 0.028 resp. p = 0.021). No statistically significant group differences were found for the following parameters: patient's age, age at diagnosis, disease duration, height, weight, condylar volume, direct and curvilinear length, medio-lateral diameters and antero-posterior diameter left.

7 Discussion

The findings of this study show that MRI recordings provide sufficient information to virtually reconstruct temporomandibular joints of JIA children in 3D using a state-of-the-art image processing software for interactive visualization. Yet the reconstruction process demands specific skills and for the time being is time consuming in order to obtain the best possible result. Magnetic resonance imaging has the advantage of non-ionizing radiation and is therefore imperative for studies on growing humans.

An initial dataset has been built for a larger cohort reflecting normal and abnormal joint development. Intra- and interindividual comparisons across three age groups could be demonstrated and quantified for different parameters. 3D-morphology in normal and deformed joints were quantitatively assessed and compared within and between subjects of different young ages. As to date, there is no MRI based quantitative data on 3D-morphology of normal and JIA diseased TMJs.

The main findings of this study suggest that during growth, especially until the age of 12, the medio-lateral diameter increases with the condylar volume, whereas the antero-posterior diameter does not change significantly. Direct and curvilinear fossa lengths increase, as the anterior fossa slope becomes steeper during formation of this anatomical feature. In severely deformed joints, steepness of the anterior fossa slope is significantly smaller, which indicates an interference during establishment of condyle-fossa-relationship. Intercondylar angle increases during growth and is smaller in condyles rated as severely deformed, also possibly because of growth

impairment and resorption effects. Resorption patterns on condyle and fossa appear to be uneven and irregular. Also an additional apposition as functional compensation is suggested by a larger antero-posterior diameter in affected condyles. The growth disturbance seems to have no connection to the general growth, as there were no differences in height or weight between subjects with no or mild joint deformation and subjects with severe joint deformation.

Descriptive 3D-reconstruction of temporomandibular joints has not yet been performed for a larger cohort and thus intra- and interindividual comparisons of 3D-reconstructions have not been possible before. In this study, it could be shown that a very detailed surface reconstruction is possible with reasonable image quality and therefore a detailed follow up of long term disease course is possible. Compared to conventional TMJ growth assessment performed only on single slices, this method offers additional aspects, namely the medio-lateral dimension and volume assessment.

So far, only a few research groups have been reconstructing mandibles or TMJs of JIA or osteoarthritis patients using CBCT (Huntjens et al., 2008; Farronato et al., 2010; Cevidanes et al., 2010). They have analyzed mandibular and/or joint asymmetry or variations in morphology. Farronato et al. came to similar results as in our work, in that they observed that the volumes of diseased condyles are significantly smaller than in the unaffected side.

To our knowledge, this study is the first one containing a larger number of joints reconstructed from MRI - and not from CBCT - as 3D-models with additional visual and quantitative assessments. Indeed, studies based on quantitative measurements of 3D-models of healthy and pathological TMJs obtained from MR images are scarce. Only one research group has so far reported on such reconstructions

of one control and one JIA patient (Kitai et al., 2002). 3D-assessment of the TMJ may ultimately provide an objective method for comparing the course of disease and effects of intervention.

Due to the nature of MRI, contrast and resolution are poorer compared to CBCT images and thus interpretation and segmentation are generally a greater challenge. In our data, image quality was poor in a few subjects due to movement artifacts at acquisition time and thus might have led to imprecise segmentation and quantification. Generally, the low geometric resolution might cause partial volume effects or irregularities. Also, the cortical border in an inflamed joint can be unclear due to acute erosive processes, yielding uncertainties during segmentation and thus resulting in differences between reconstructed and actual joint morphology. However, MRI, as a non-ionizing imaging method offers an ethically acceptable harmless procedure – especially in growing subjects - with sufficiently informative results.

The TMJ has a broadly variable morphology. There is no established control study to determine normal quantitative anatomical parameters. A standardized "healthy" TMJ model has never been defined and is probably undefinable also due to remodelling effects. JIA might however cause an even broader geometric variation and irregular shapes which make intra- and interindividual comparisons challenging, unlike in the hip joint. Due to the fluctuation of erosive and reparative phases of JIA, the total number of affected joints in this study was not absolutely certain, unilateral involvement is being reported generally in 30 - 50% of cases. Furthermore, inter-individual comparability is hampered by genetic and other possible developmental factors. Finally, since most of the subjects had received treatment before MR imaging (in round 60% DMARDs, disease-

modifying anti-rheumatic drugs) we cannot fully exclude that this might also have influenced the outcome. Therefore, larger better defined cohorts, distributed over different age groups and including healthy controls, are desirable and would increase the statistical power and improve results interpretation.

At first, a quantitative assessment of CT datasets and/or cadaver sections should be compared to MRI reconstructions in order to assess the accuracy of the segmentation procedure and validate it. Subsequently, a pool of 3D normative data across the growth period until adult age should be collected from MR image series, ideally statically as well as in function. Joint space assessment, possibly dynamically as well (dynamic stereometry), and volumetric quantization of joint fluid would add further valuable information (Gössi et al., 2004; Gallo et al., 2000, 2006; Ettlin et al., 2008). Thus, longitudinal assessment of TMJ growth, possibly including the whole mandible, would help clinicians to establish an early and accurate diagnosis of TMJ involvement in children with JIA, to follow-up the patients in the long term and to gain new insights on treatment effects.

8 Conclusion

This study shows that 3D-reconstructions from MR images of TMJs of children with JIA are feasible and provide useful information for the visual and quantitative assessment of joint morphology. Indeed, during growth, the condylar diameter increases medio-laterally, whereas it does not change antero-posteriorly. Also, during growth, the fossa becomes deeper and the intercondylar angle larger. In severely deformed TMJs however, the fossa remains shallower with a smaller intercondylar angle.

The use of magnetic fields avoids exposure to ionizing radiation and is ethically suitable for growing persons. Yet the reconstruction process demands specific skills and for the time being is time consuming in order to obtain the best possible result.

A collection of a larger cohort of accurately chosen patients and controls followed over a longer time period shall provide a more complete database helpful for the clinicians to better interpret involvement and severity of TMJs of JIA patients.

9 Tables

Cells containing extreme values (maxima and minima) are shaded in grey.

Table 9.1. Subject demographic data and characteristics

Subject	Gender	Age at examination [years]	Age at diagnosis [years]	Disease duration [years]	Height [cm]	Weight [kg]	Diagnosis	RF	ANA	HLA B27	Uveitis
1	f	11.1	6.8	4.2	147.2	47.8	oligo	neg	pos	?	pos
2	m	8.5	2.5	5.9	132.0	29.0	poly	neg	neg	neg	neg
3	m	7.9	7.3	0.7	128.0	25.5	pso	neg	pos	neg	neg
4	f	6.6	6.5	0.1	117.5	19.0	oligo	neg	neg	neg	neg
5	f	4.7	4.6	0.1	107.0	17.9	oligo	neg	pos	pos	neg
6	m	12.2	12.1	0.1	147.5	33.2	poly	neg	pos	neg	neg
7	f	9.7	1.0	8.7	143.0	32.0	poly	neg	neg	neg	neg
8	f	7.9	3.1	4.8	121.6	23.3	poly	neg	pos	neg	neg
9	f	13.3	4.3	9.0	150.5	39.9	oligo ext	neg	pos	neg	neg
10	f	6.2	3.7	2.6	120.0	21.0	poly	neg	pos	neg	pos
11	f	8.3	6.8	1.5	127.0	26.4	poly	neg	neg	neg	neg
12	m	3.8	3.3	0.4	109.0	19.0	oligo	neg	neg	neg	neg
13	f	11.5	11.0	0.5	152.0	44.9	oligo	neg	pos	neg	neg
14	m	11.8	7.1	4.7	146.9	36.1	ERA	neg	pos	neg	neg
15	m	6.9	5.2	1.6	118.0	22.0	oligo	neg	neg	neg	neg
16	m	11.8	11.8	0.1	138.0	31.2	poly	neg	pos	neg	neg
17	m	10.5	5.5	5.0	139.8	29.7	oligo	neg	pos	neg	neg
18	f	4.4	1.7	2.7	104.0	15.2	oligo ext	neg	pos	neg	pos
19	f	16.9	14.1	2.8	163.0	61.0	poly	neg	pos	neg	neg
20	f	7.7	2.8	4.9	126.0	26.0	oligo	neg	pos	neg	neg
21	f	5.3	3.4	1.9	?	16.0	poly	neg	pos	?	neg
22	m	11.6	8.3	3.3	157.0	37.6	oligo ext	neg	pos	neg	neg
23	m	15.6	3.4	12.2	166.3	46.8	poly	neg	pos	neg	neg
24	f	10.4	9.7	0.7	151.3	42.4	ERA	neg	neg	neg	neg
25	m	2.7	1.1	1.6	96.3	14.6	oligo	neg	neg	?	neg
26	m	4.7	2.5	2.3	116.7	23.3	poly	neg	pos	neg	neg
27	m	10.7	9.9	0.9	142.8	34.4	ERA	neg	neg	neg	neg
28	f	11.4	8.4	2.9	144.0	33.9	oligo	neg	pos	neg	pos
median		9.1	5.4	2.5	138.0	29.4					
mean ± SD		9.1 ± 3.6	6.0 ± 3.6	3.1 ± 3.0	133.8 ± 18.8	30.3 ± 11.4					

Table 9.2. Intercondylar angle

Subject	Angle [°]
1	138.6
2	150.6
3	143.8
4	140
5	134.3
6	136
7	150
8	141.6
9	140.3
10	144.5
11	158
12	129.1
13	139.5
14	146.6
15	151.9
16	151.5
17	140.5
18	124.5
19	136.8
20	142.9
21	127.4
22	146.7
23	138.2
24	139.7
25	147.8
26	128.1
27	146.8
28	119.7
median	140.4
mean ± SD	140.6 ± 8.8

Table 9.3. Condylar volume

Subject	Volume R [mm³]	Volume L [mm³]	Ratio
1	674	725	1.08
2	1013	965	1.05
3	1382	1036	1.33
4	506	600	1.19
5	618	565	1.09
6	702	610	1.15
7	786	849	1.08
8	616	650	1.06
9	968	1106	1.14
10	641	645	1.01
11	718	677	1.06
12	654	807	1.23
13	859	798	1.08
14	827	714	1.16
15	744	740	1.01
16	613	703	1.15
17	720	794	1.10
18	537	553	1.03
19	889	1042	1.17
20	693	796	1.15
21	481	572	1.19
22	787	929	1.18
23	1018	787	1.29
24	526	564	1.07
25	405	498	1.23
26	329	425	1.29
27	788	1084	1.38
28	546	376	1.45
median	697.5	719.5	1.15
mean ± SD	715.7 ± 215.2	736.1 ± 194.4	1.16 ±0.11

Table 9.4. Steepness of the anterior fossa slope

Subject	Steepness R (parasagittal) [°]	Steepness L (parasagittal) [°]	Steepness R (sagittal) [°]	Steepness L (sagittal) [°]
1	43.7	43.1	30.1	31.4
2	28.8	29.8	34.3	42.8
3	36.1	40.5	36.2	31.5
4	30.6	28.3	30.5	27.4
5	23.6	26.1	21.4	20.2
6	15.8	24.5	9.8	21.8
7	35.3	34.0	35.0	33.3
8	26.7	25.3	23.5	20.2
9	46.5	49.7	42.3	47.2
10	39.4	36.5	39.8	34.1
11	33.2	35.4	33.9	34.6
12	27.1	22.5	23.1	18.4
13	28.1	29.1	28.0	26.1
14	29.9	36.6	32.5	38.2
15	40.5	45.5	38.6	45.0
16	38.6	48.5	38.5	44.7
17	35.9	34.8	35.4	34.3
18	14.3	12.9	13.1	9.5
19	33.7	25.1	36.2	25.4
20	32.8	36.1	33.7	35.9
21	28.7	18.6	19.7	9.4
22	40.1	38.1	34.3	35.7
23	31.3	22.4	20.3	19.9
24	31.8	32.7	30.7	32.7
25	14.3	14.1	2.5	8.9
26	23.1	28.2	22.3	20.8
27	32.2	33.0	28.9	31.9
28	21.3	20.1	25.5	15.9
median	31.6	31.3	30.6	31.5
mean ± SD	30.8 ± 8.3	31.1 ± 9.6	28.6 ± 9.5	28.5 ± 10.8

Table 9.5. Direct length of the anterior fossa slope

Subject	Length R (parasagittal) [mm]	Length L (parasagittal) [mm]	Length R (sagittal) [mm]	Length L (sagittal) [mm]
1	8.8	9.1	11.2	10.5
2	10.4	11.7	12.0	15.7
3	10.3	9.2	10.1	9.8
4	9.7	9.0	9.7	9.5
5	10.3	10.1	10.3	9.6
6	9.9	12.3	9.0	10.5
7	12.0	12.3	12.1	12.7
8	13.4	13.1	16.4	13.2
9	12.8	12.4	13.7	12.7
10	11.6	12.7	11.5	13.2
11	10.4	9.5	10.5	9.5
12	7.5	7.5	7.5	6.1
13	8.9	9.2	8.9	10.1
14	12.0	10.9	11.3	10.8
15	13.3	12.0	14.5	12.3
16	10.8	9.8	10.6	10.5
17	15.4	16.2	14.7	14.6
18	9.2	11.7	10.2	10.8
19	12.5	11.9	13.9	12.3
20	12.2	10.8	12.5	12.9
21	9.7	9.7	9.5	9.5
22	13.8	13.9	15.3	14.8
23	11.9	9.3	11.7	9.1
24	11.8	12.3	12.6	12.1
25	6.0	7.2	3.9	4.8
26	12.5	10.6	10.4	9.9
27	12.0	12.9	13.7	13.0
28	11.2	11.6	11.0	9.8
median	11.4	11.2	11.2	10.6
mean ± SD	11.1 ± 2.0	11.0 ± 2.0	11.4 ± 2.6	11.1 ± 2.4

Table 9.6. Curvilinear length of the anterior fossa slope

Subject	Curv R (parasagittal) [mm]	Curv L (parasagittal) [mm]	Curv R (sagittal) [mm]	Curv L (sagittal) [mm]
1	10.0	9.6	13.5	11.4
2	11.4	12.0	12.3	17.2
3	10.6	10.0	10.9	11.0
4	10.2	9.4	10.4	10.2
5	10.8	10.3	10.3	10.5
6	10.6	14.5	9.2	10.1
7	13.7	13.3	12.9	12.8
8	13.2	13.5	16.9	13.7
9	14.2	14.2	14.7	14.4
10	14.1	13.6	12.2	12.0
11	10.1	10.0	11.2	11.1
12	6.3	7.6	8.2	7.7
13	10.4	9.5	9.1	9.2
14	11.7	11.7	12.3	12.9
15	13.0	13.1	15.3	14.5
16	12.0	11.2	11.7	11.5
17	15.4	17.3	15.9	16.4
18	10.9	11.9	10.1	9.3
19	12.4	12.0	14.5	13.0
20	13.8	12.1	13.7	13.4
21	9.3	9.8	9.6	9.9
22	15.9	15.0	17.0	15.5
23	10.0	9.4	11.9	12.0
24	13.0	13.1	13.1	12.6
25	4.8	7.2	6.1	6.0
26	10.1	11.0	10.6	12.7
27	13.6	13.7	14.0	12.6
28	10.0	11.8	11.2	11.2
median	11.2	11.9	12.1	12.0
mean ± SD	11.5 ± 2.5	11.7 ± 2.3	12.1 ± 2.6	12.0 ± 2.5

Table 9.7. Medio-lateral (MLD) and antero-posterior diameter (APD) of the condyles

Subject	MLD R [mm]	MLD L [mm]	APD R [mm]	APD L [mm]
1	18.2	17.4	7.2	8.4
2	17.7	15.8	7.9	8.3
3	15.3	15.2	6.5	7.0
4	13.5	14.6	6.1	7.0
5	14.7	13.1	7.7	7.4
6	11.1	10.4	11.1	11.8
7	15.9	13.8	6.7	7.4
8	15.5	15.6	8.7	9.1
9	16.5	16.1	8.4	7.7
10	13.5	13.4	7.6	7.7
11	16.1	16.0	7.9	8.8
12	13.4	13.2	6.7	7.6
13	14.8	15.1	7.9	7.4
14	16.4	16.1	5.9	5.1
15	17.6	16.6	8.1	8.3
16	16.6	16.7	6.2	5.7
17	14.3	14.1	7.7	7.3
18	10.7	11.0	8.2	8.0
19	16.6	16.5	7.1	7.9
20	18.2	17.5	7.6	7.5
21	15.5	15.8	6.3	7.1
22	16.6	17.3	7.9	7.7
23	18.4	16.1	8.9	8.7
24	14.2	14.9	8.0	7.6
25	12.1	12.4	7.4	7.6
26	13.0	13.9	7.2	7.9
27	15.6	16.4	7.0	8.1
28	16.6	14.0	10.0	6.2
median	15.6	15.4	7.7	7.7
mean ± SD	15.3 ± 2.1	15.0 ± 1.8	7.6 ± 1.1	7.7 ± 1.2

Table 9.8. MRI gradation

Subject	Deformation R	Deformation L	Enhancement R	Enhancement L	Joint fluid R	Joint fluid L
1	no	no	normal	normal	normal	normal
2	mild	mild	prominent	prominent	normal	increased
3	no	no	normal	normal	normal	normal
4	no	no	normal	normal	normal	normal
5	no	no	prominent	normal	normal	normal
6	severe	severe	increased	increased	increased	normal
7	no	no	normal	normal	normal	normal
8	severe	severe	normal	normal	increased	increased
9	severe	severe			normal	increased
10	no	no	prominent	prominent	normal	normal
11	no	no	normal	normal	normal	normal
12	no	no	prominent	prominent	normal	normal
13	no	no	normal	normal	normal	normal
14	no	no	prominent	normal	normal	normal
15	no	no	prominent	prominent	normal	normal
16	no	no	prominent	normal	normal	normal
17	no	no	normal	normal	normal	normal
18	severe	severe	increased	increased	normal	normal
19	no	no	normal	normal	normal	normal
20	mild	no	increased	prominent	normal	normal
21	no	severe	prominent	increased	normal	normal
22	no	no	normal	normal	normal	normal
23	no	severe	normal	increased	normal	increased
24	no	no	prominent	normal	normal	normal
25	no	no	prominent	prominent	normal	normal
26	no	no	normal	normal	normal	normal
27	no	no	normal	normal	normal	normal
28	severe	severe	prominent	increased	normal	normal

Table 9.9. Group A. No or mild joint deformation.

Subject	Deformation R	Deformation L
1	no	no
2	mild	mild
3	no	no
4	no	no
5	no	no
7	no	no
10	no	no
11	no	no
12	no	no
13	no	no
14	no	no
15	no	no
16	no	no
17	no	no
19	no	no
20	mild	no
21	no	
22	no	no
23	no	
24	no	no
25	no	no
26	no	no
27	no	no

Table 9.10. Group B. Severe deformation.

Subject	Deformation R	Deformation L
6	severe	severe
8	severe	severe
9	severe	severe
18	severe	severe
21	no	severe
23	no	severe
28	severe	severe

Table 9.11. Comparison of three age groups using nonparametric Kruskal-Wallis test

*(n.s. = non significant, * p = 0.05, ** p = 0.01, *** p = 0.001)*

	Mean	Std. deviation	Median	Minimum	Maximum	p	Significance level
Age at diagnosis	5.996	3.5918	5.350	1.0	14.1	0.025	*
Disease duration	3.079	3.0212	2.450	0.1	12.2	0.271	n.s.
Height	133.79	18.754	138.00	96	166	0	***
Weight	30.325	11.3884	29.350	14.6	61.0	0.001	**
Intercondylar angle	140.550	8.9837	140.400	119.7	158.0	0.008	**
Condylar volume	725.89	194.265	715.00	377	1209	0.007	**
Steepness parasagittal	30.980	8.6123	30.850	13.6	48.1	0.003	**
Steepness sagittal	28.523	9.7925	30.775	5.7	44.8	0.003	**
Direct length	11.139	2.0943	10.886	5.5	15.2	0.047	*
Curvilinear length	11.812	2.2847	11.355	6.0	16.3	0.009	**
MLD L	14.959	1.8402	15.405	10.4	17.5	0.023	*
MLD R	15.301	2.0706	15.575	10.7	18.4	0.017	*
APD L	7.715	1.1733	7.665	5.1	11.8	0.153	n.s.
APD R	7.635	1.1448	7.655	5.9	11.1	0.148	n.s.

Table 9.12. Bonferroni post-hoc comparisons

Group 1: age between 0 and 6 years
Group 2: age between 6 and 12 years
Group 3: age between 12 and 18 years

	1 and 2	1 and 3	2 and 3
Age at diagnosis	0.074	0.037 *	0.833
Height	<0.001 ***	<0.001 ***	0.018 *
Weight	0.009 **	<0.001 ***	0.012 *
Intercondylar angle	0.01 *	0.832	0.333
Condylar volume	0.058	0.015 *	0.446
Steepness parasagittal	0.001 **	0.076	1.000
Steepness sagittal	<0.001 ***	0.043 *	0.543
Direct length	0.016 *	0.113	1.000
Curvilinear length	0.009 **	0.084	1.000
MLD L	0.004	0.182	1.000
MLD R	0.008	0.086	1.000

Table 9.13. Comparison between groups A and B using nonparametric U test

*(n.s. = non significant, * p = 0.05, ** p = 0.01, *** p = 0.001)*

	Mean	Std. deviation	Median	Minimum	Maximum	p	Significance level
Age at examination	9.075	3.5612	9.100	2.7	16.9	.367	n. s.
Age at diagnosis	5.996	3.5918	5.350	1.0	14.1	.542	n. s.
Disease duration	3.079	3.0212	2.450	.1	12.2	.184	n. s.
Height	133.79	18.754	138.00	96	166	.382	n. s.
Weight	30.325	11.3884	29.350	14.6	61.0	.958	n. s.
Intercondylar angle	140.550	8.9837	140.400	119.7	158.0	.009	**
Condylar volume	725.89	194.265	715.00	377	1209	.313	n. s.
Steepness parasagittal	30.980	8.6123	30.850	13.6	48.1	.028	*
Steepness sagittal	28.523	9.7925	30.775	5.7	44.8	.021	*
Direct length	11.139	2.0943	10.886	5.5	15.2	.853	n. s.
Curvilinear length	11.812	2.2847	11.355	6.0	16.3	.811	n. s.
MLD L	14.959	1.8402	15.405	10.4	17.5	.353	n. s.
MLD R	15.301	2.0706	15.575	10.7	18.4	.894	n. s.
APD L	7.715	1.1733	7.665	5.1	11.8	.222	n. s.
APD R	7.635	1.1448	7.655	5.9	11.1	.003	**

10 Figures

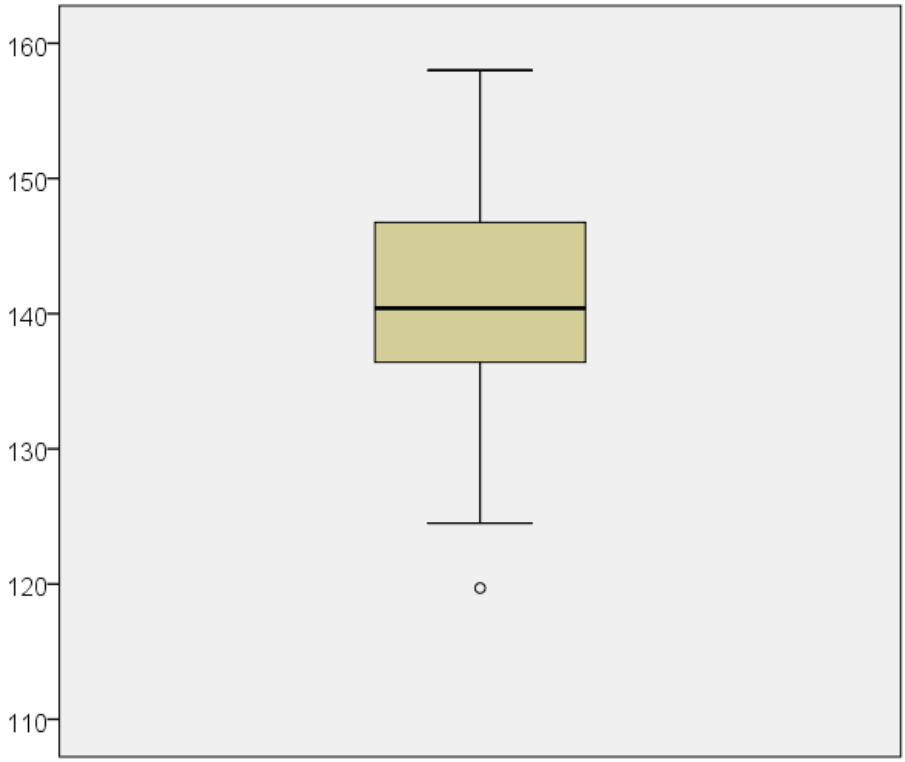

Figure 10.1. Box plot showing intercondylar angle

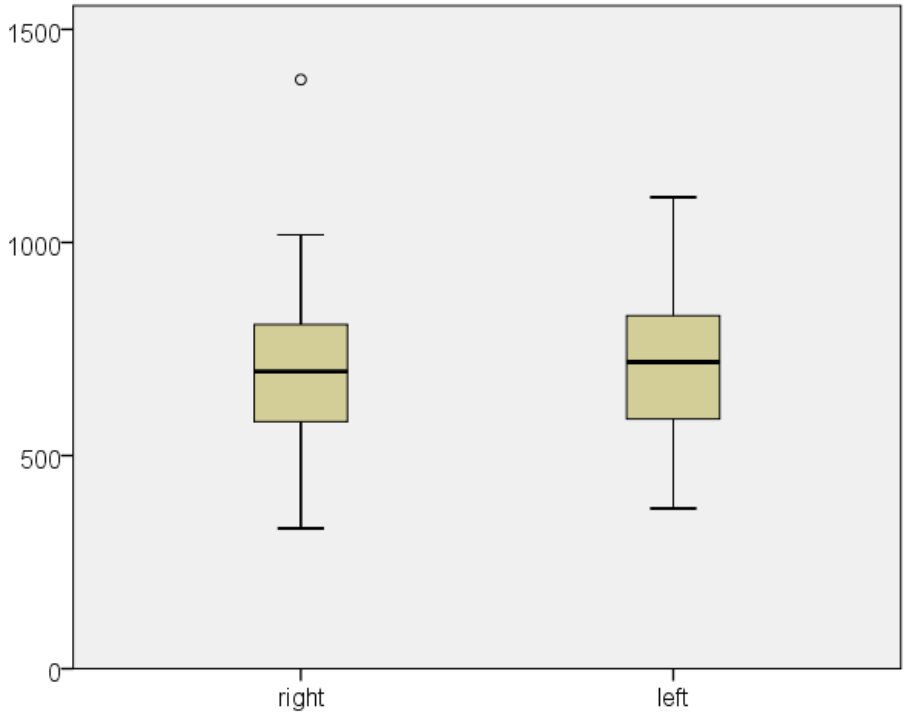

Figure 10.2. Box plot showing volumes for both condyles

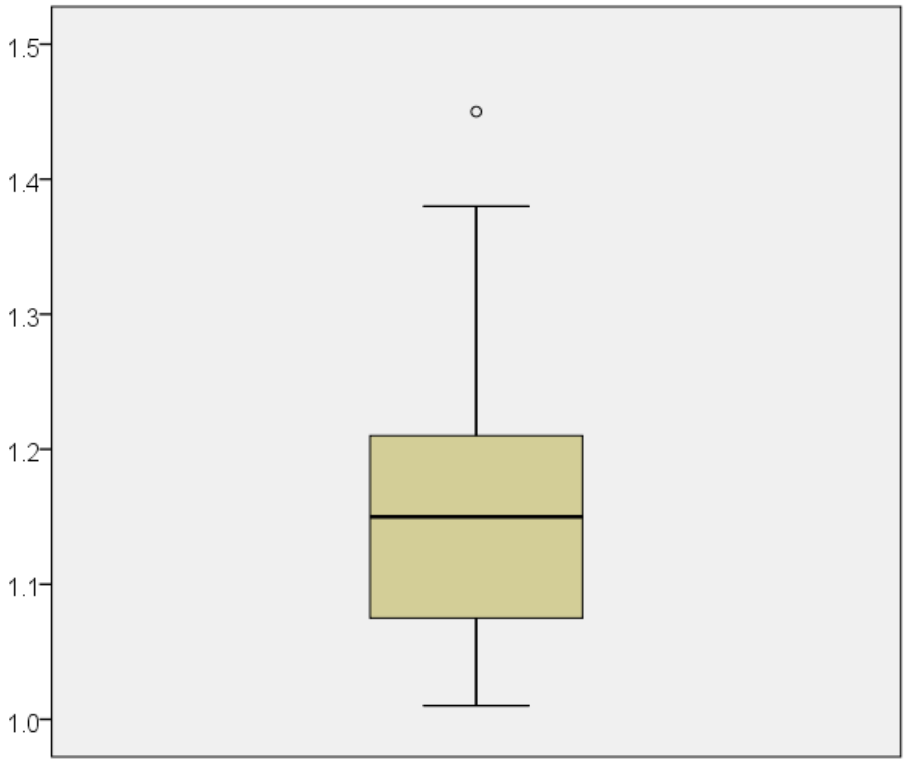

Figure 10.3. Box plot showing condylar volume ratio

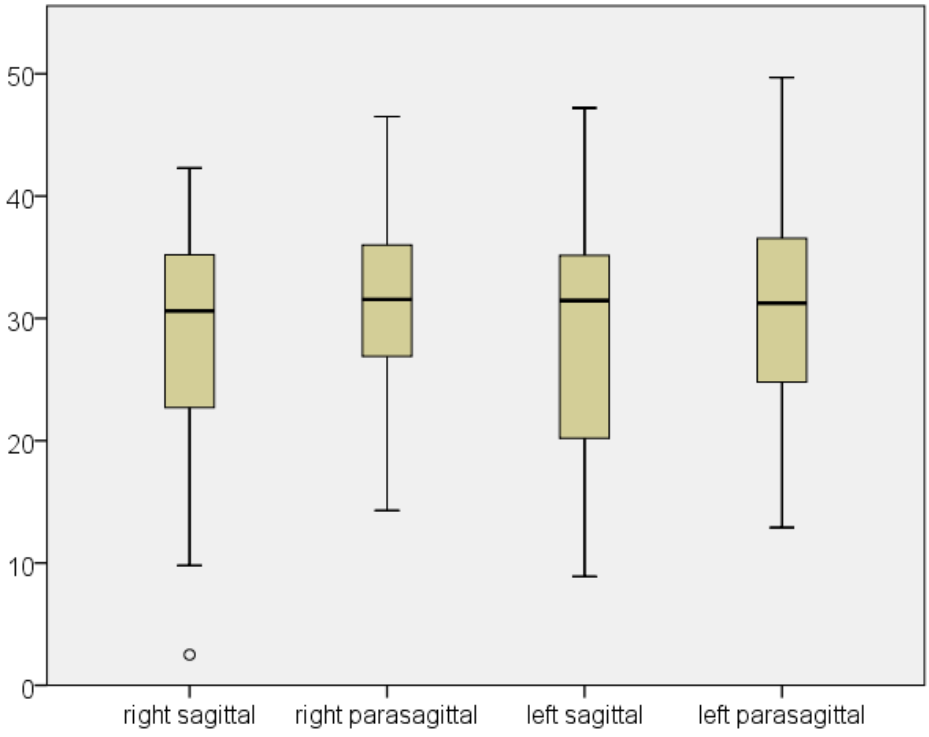

Figure 10.4. Box plot showing steepness of the anterior fossa slope

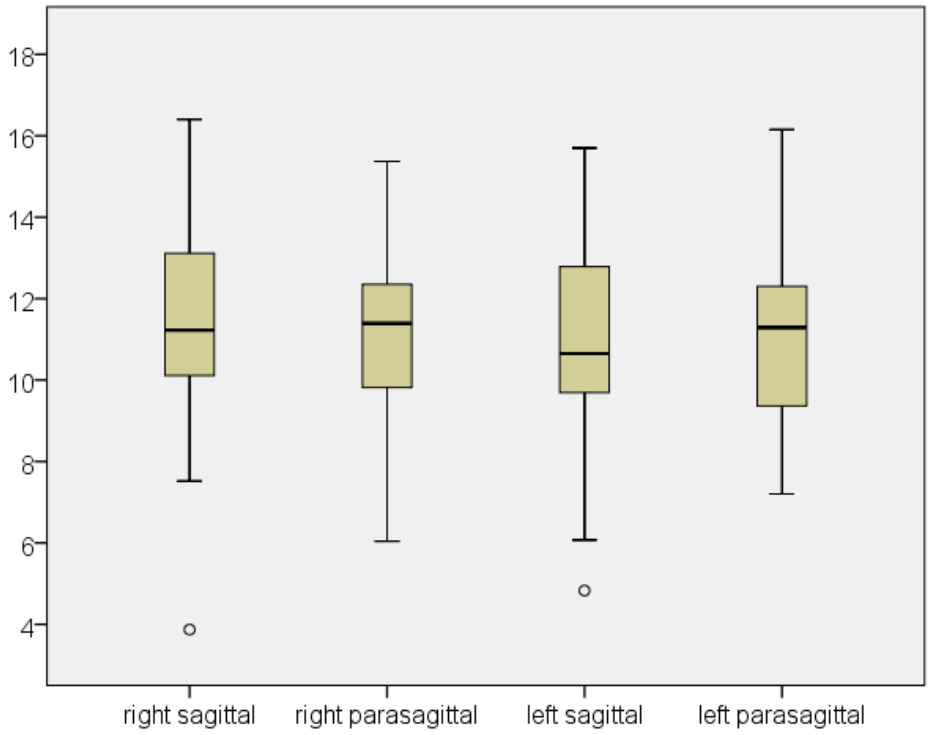

Figure 10.5. Box plot showing direct length of the anterior fossa slope

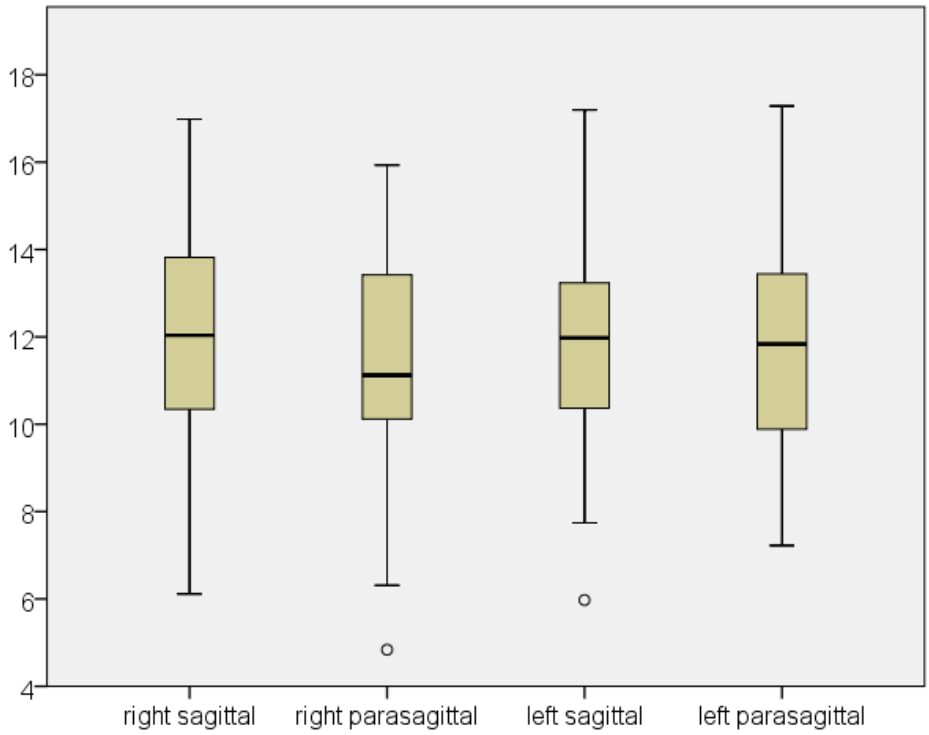

Figure 10.6. Box plot showing curvilinear length of the anterior fossa slope

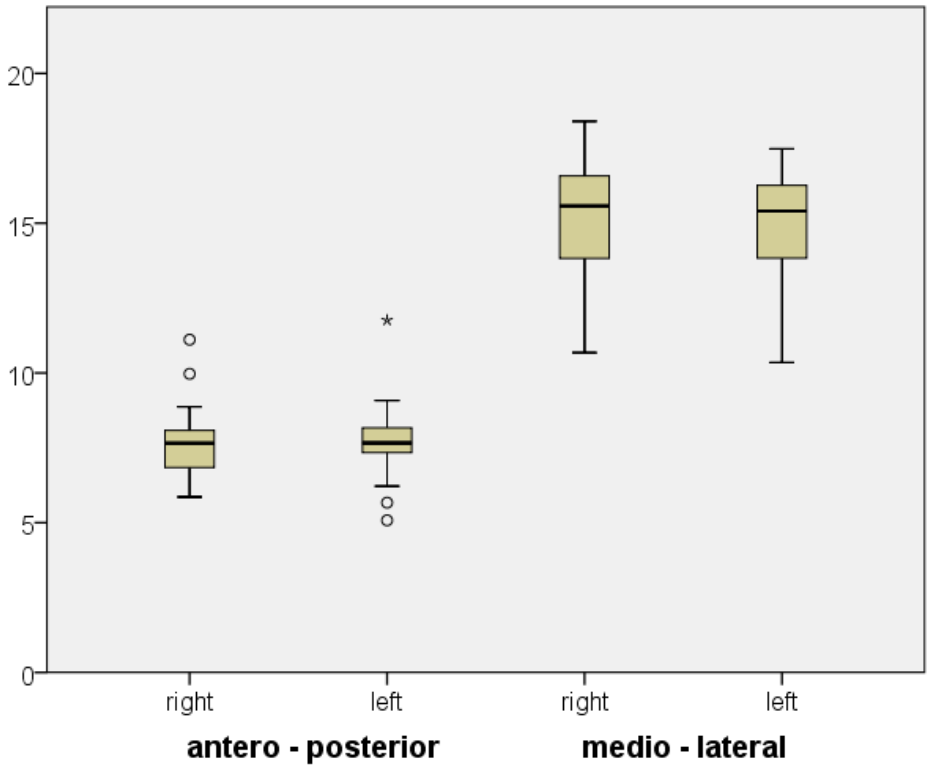

Figure 10.7. Box plot showing antero-posterior and medio-lateral diameters of both condyles

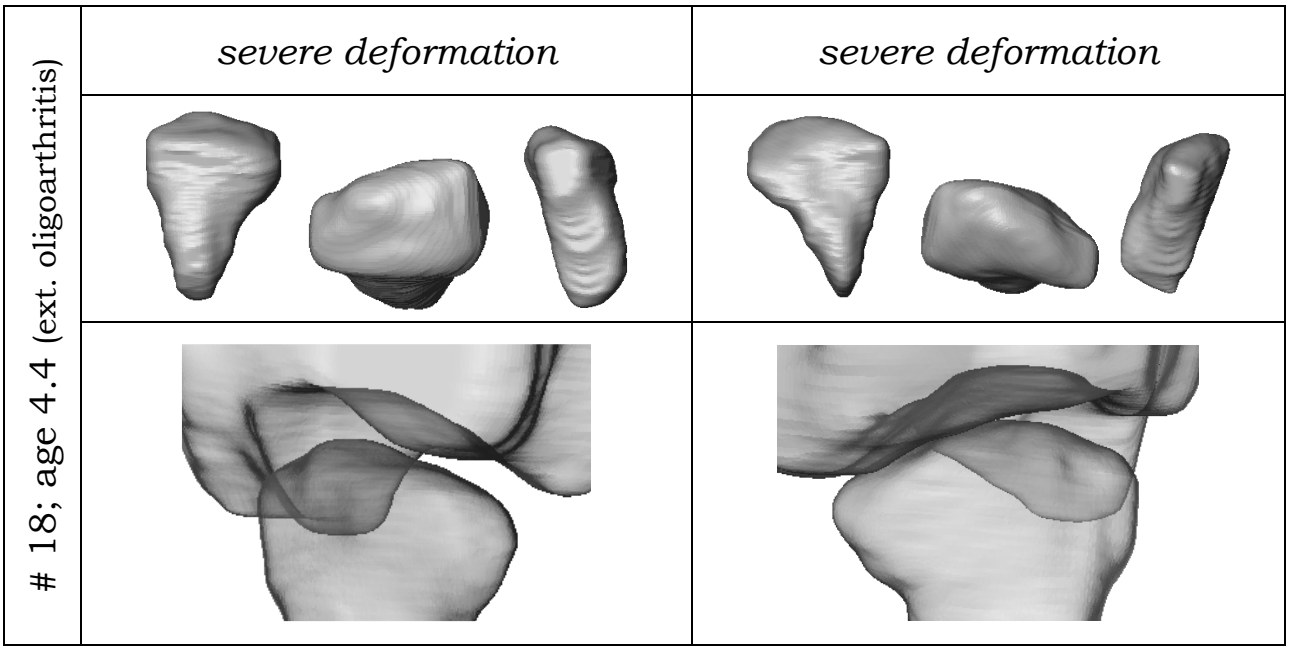

Figure 10.8. Subject no. 18 (age: 4.4 years), graded as both condyles with severe deformation

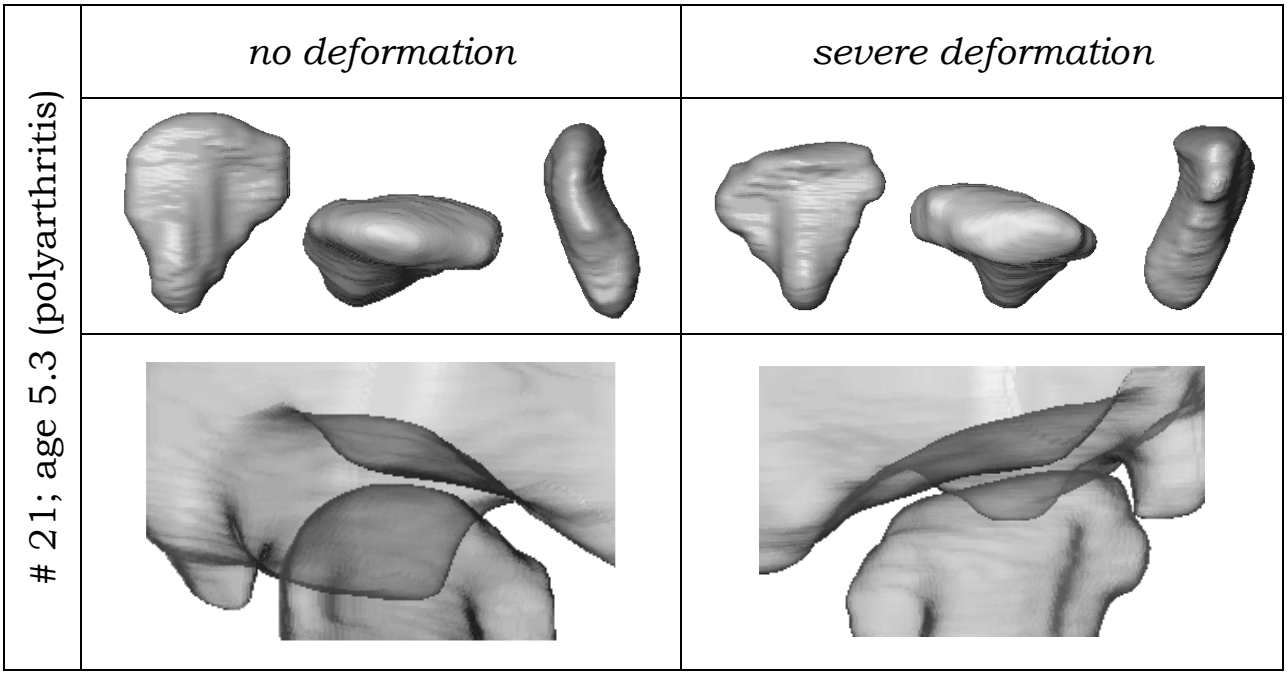

Figure 10.9. Subject no. 21 (age: 5.3 years), graded as right condyle with no deformation and left condyle with severe deformation

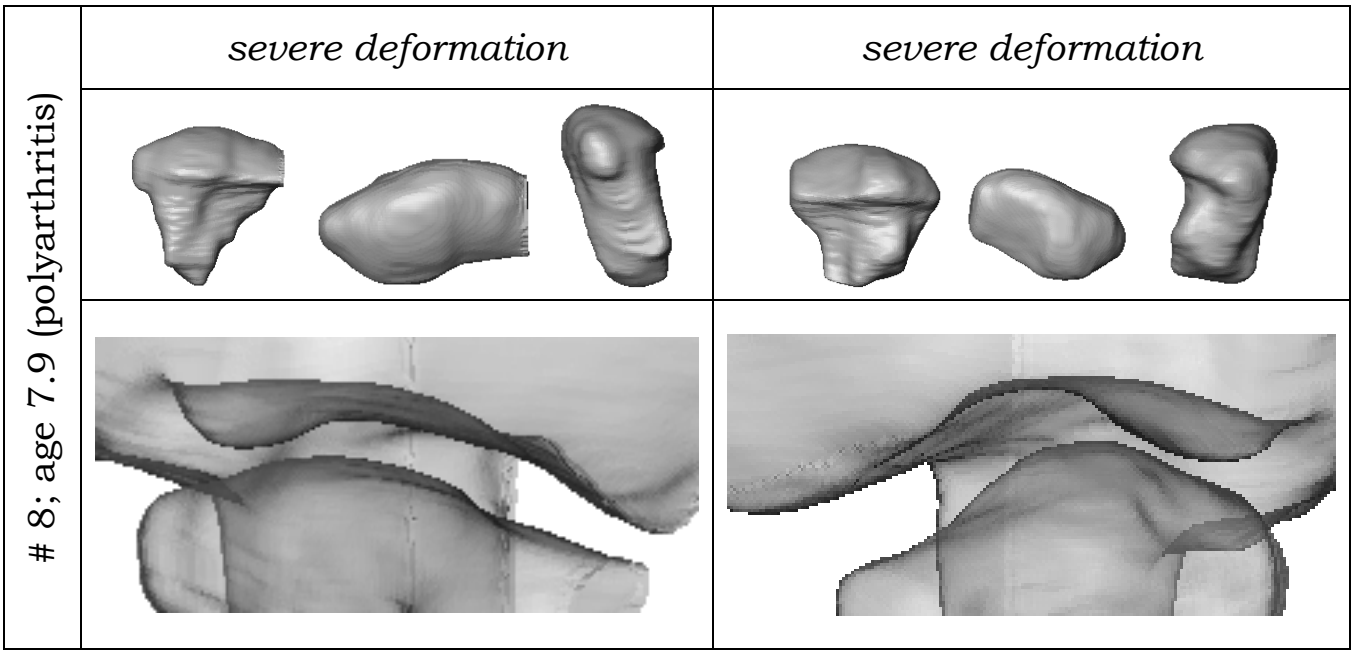

Figure 10.10. Subject no. 8 (age: 7.9 years), graded as both condyles with severe deformation

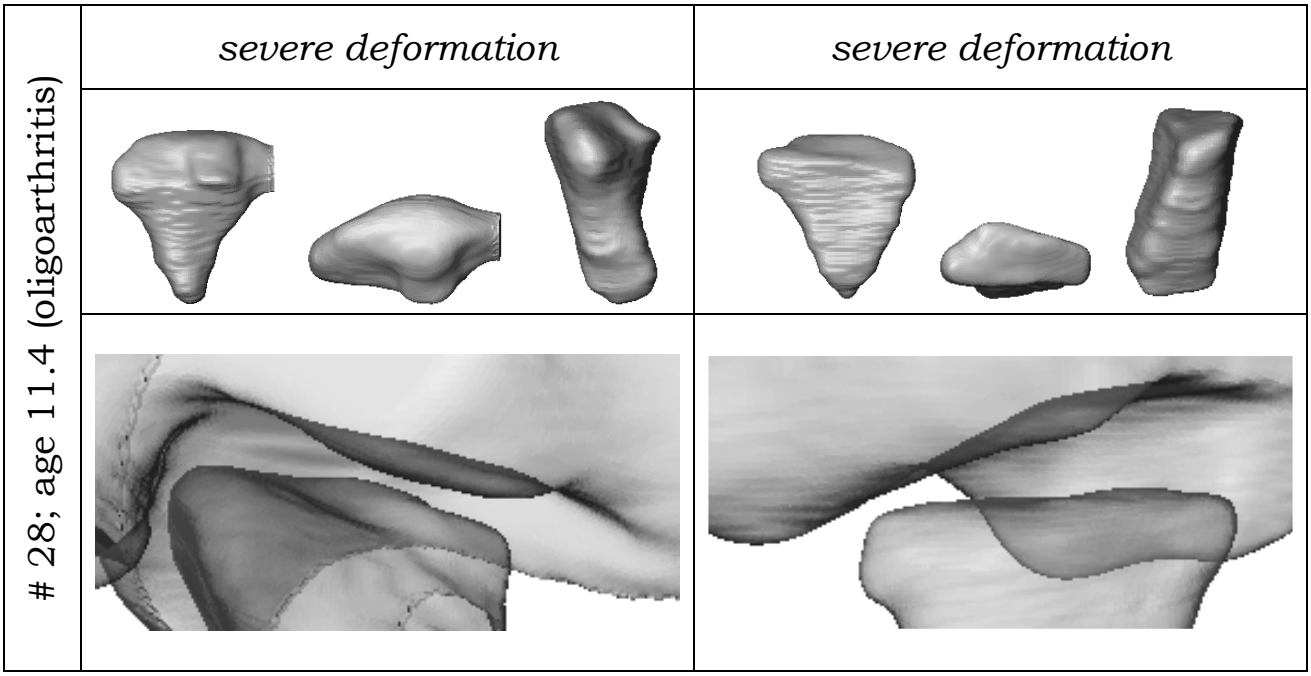

Figure 10.11. Subject no. 28 (age: 11.4 years), graded as both condyles with severe deformation

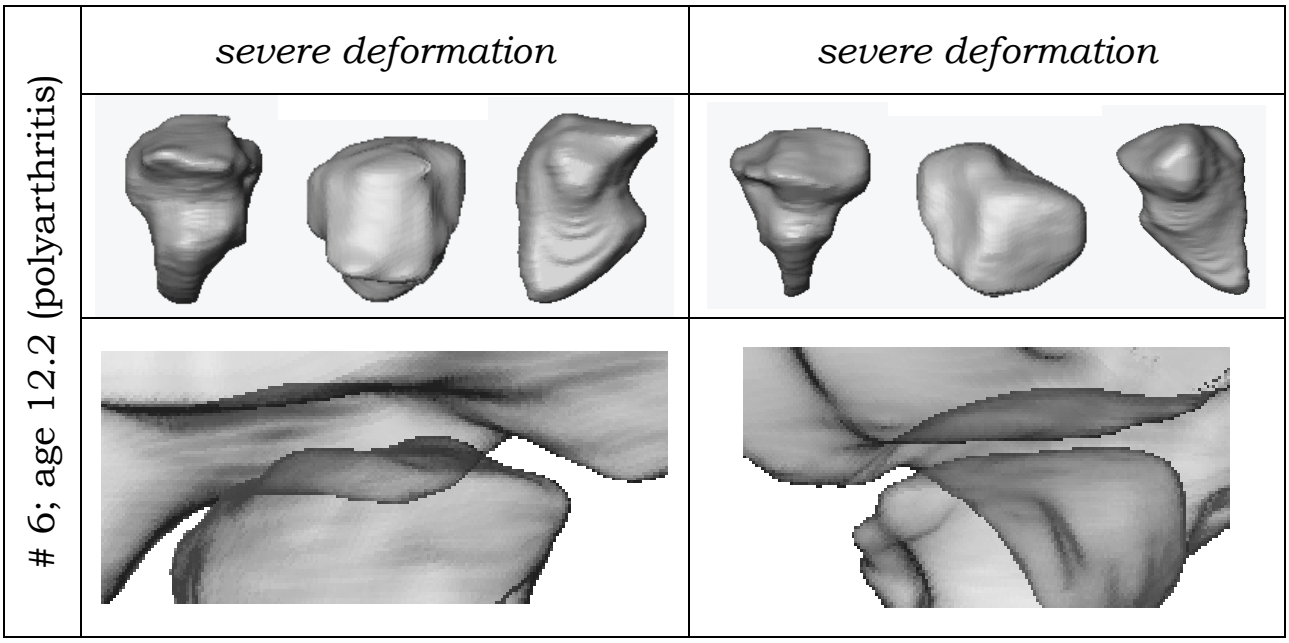

Figure 10.12. Subject no. 6 (age: 12.2 years), graded as both condyles with severe deformation

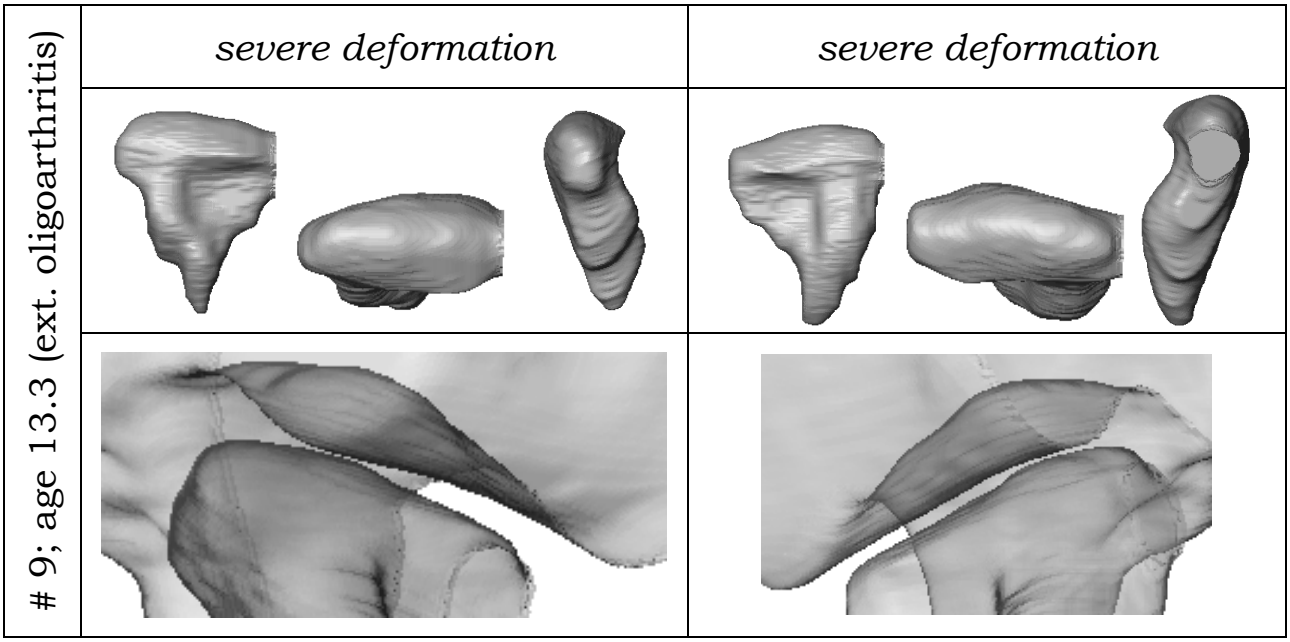

Figure 10.13. Subject no. 9 (age: 13.3 years), graded as both condyles with severe deformation

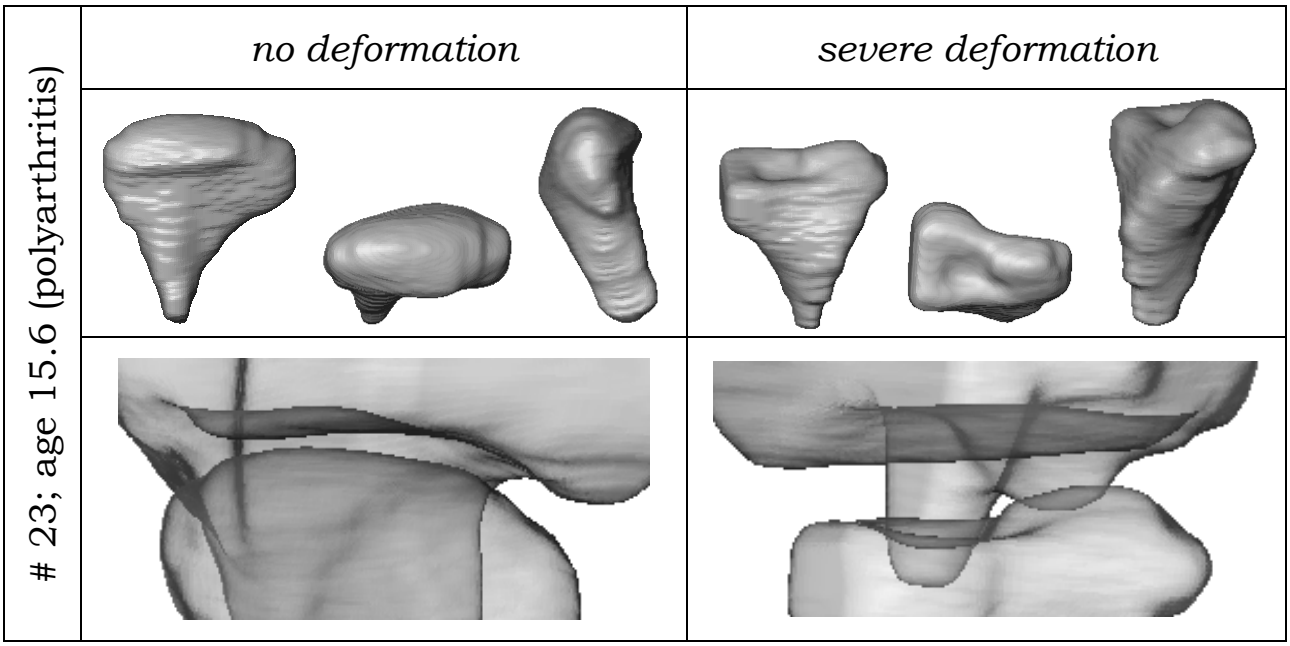

Figure 10.14. Subject no. 23 (age: 15.6 years), graded as right condyle with no deformation and left condyle with severe deformation

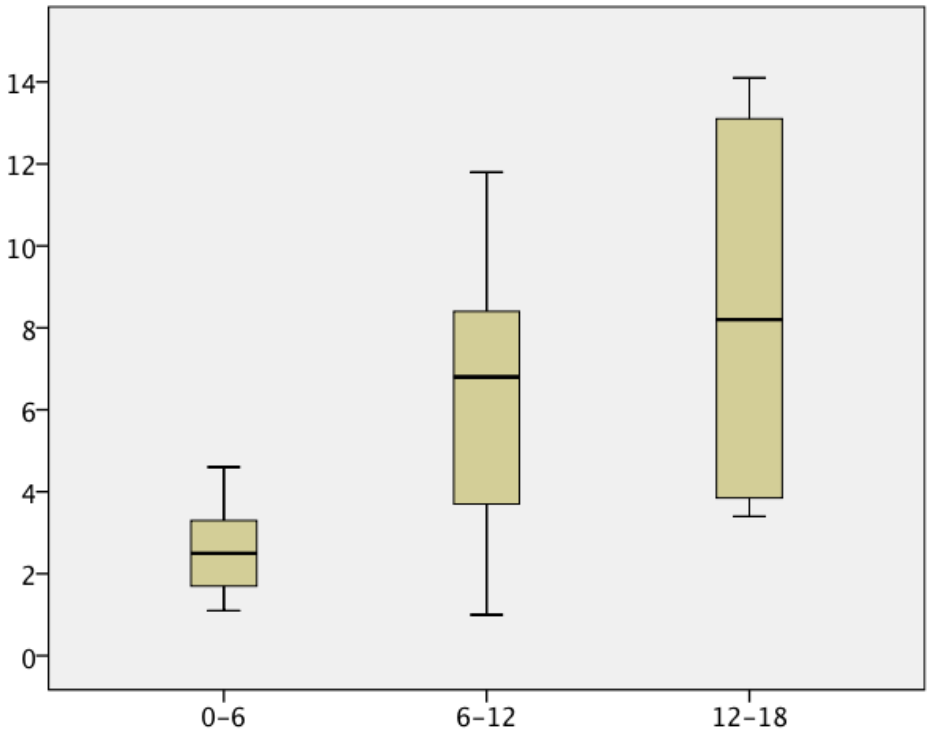

Figure 10.15. Comparison of age at diagnosis among the three age groups

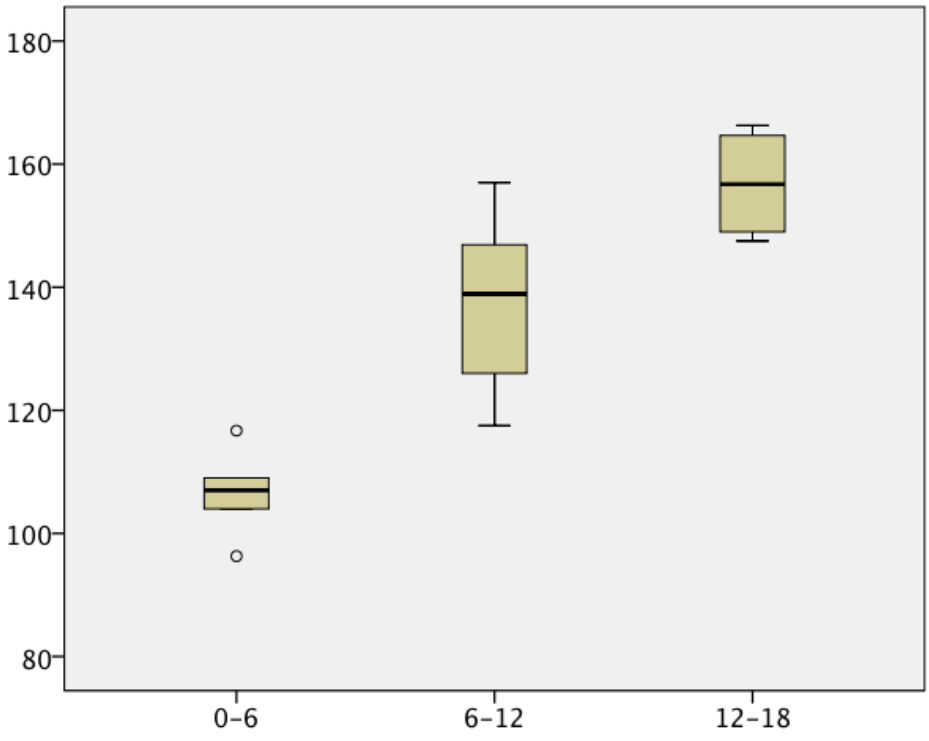

Figure 10.16. Height comparison among the three age groups

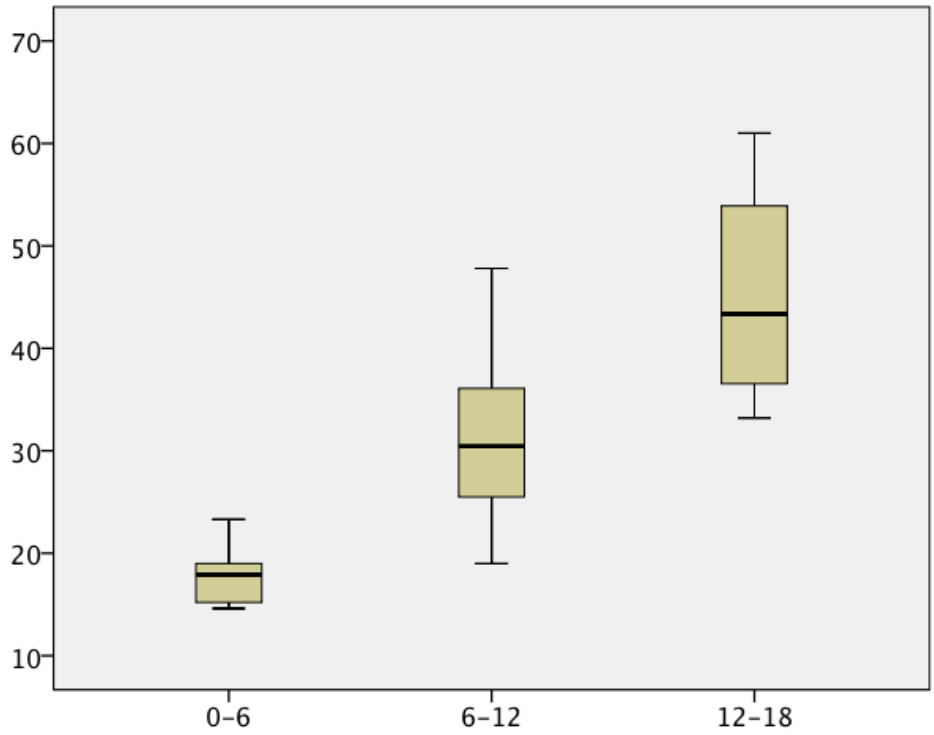

Figure 10.17. Weight comparison among the three age groups

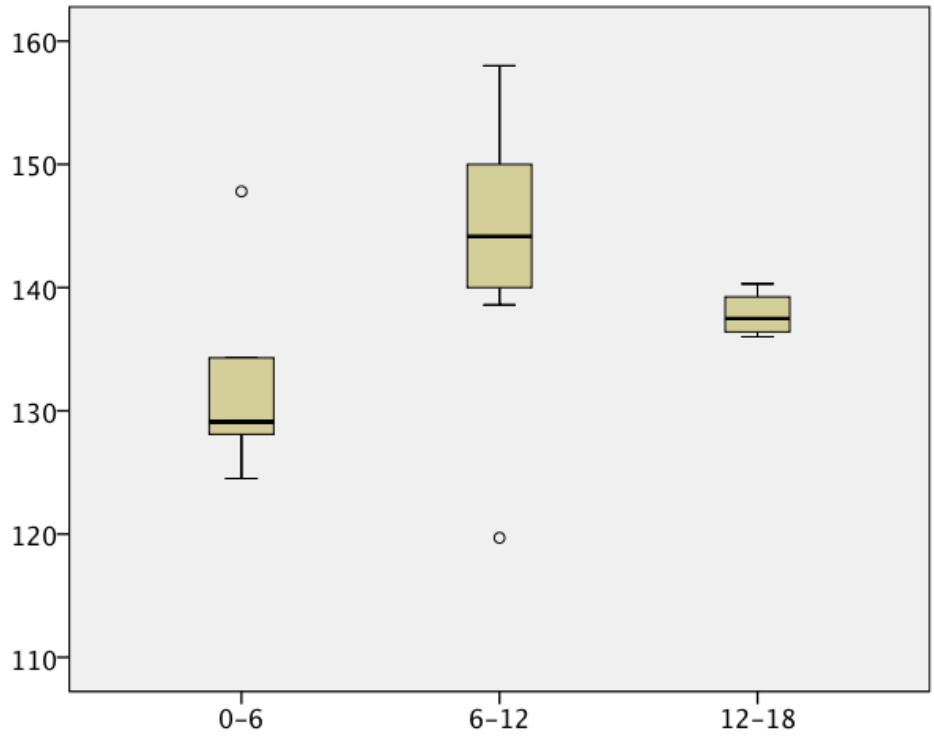

Figure 10.18. Intercondylar angle comparison among the three age groups

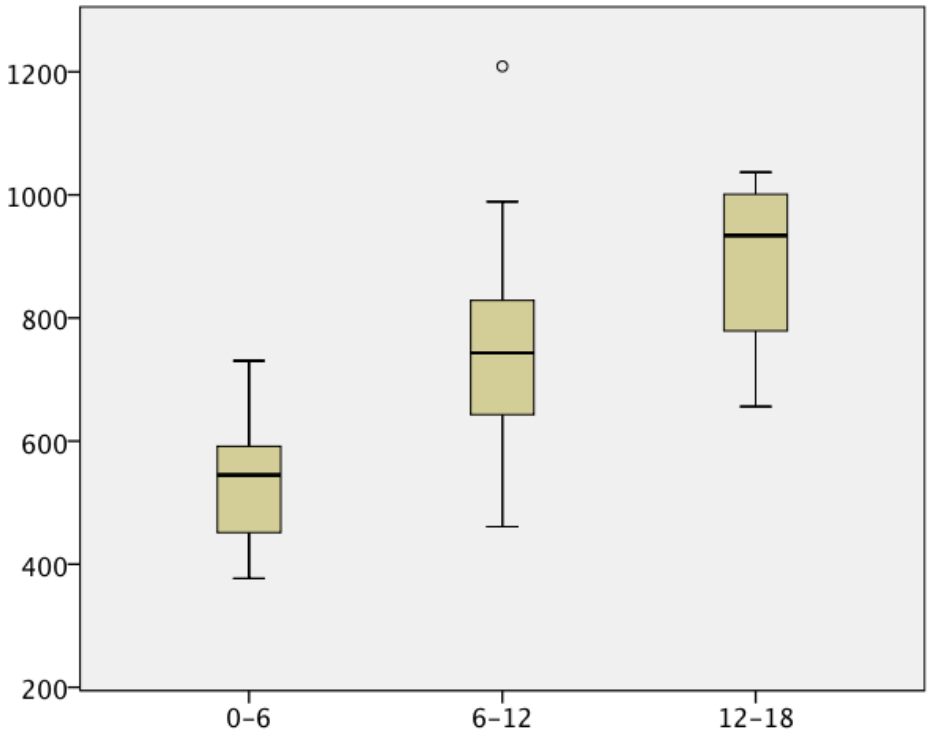

Figure 10.19. Condylar volume comparison among the three age groups

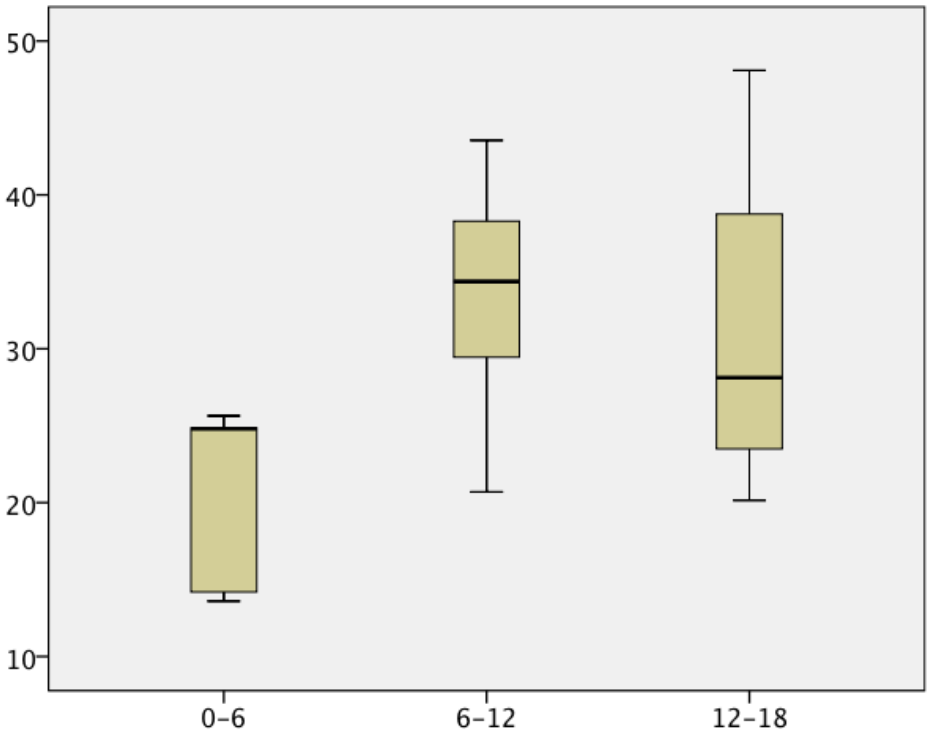

Figure 10.20. Comparison of steepness of anterior fossa slope in parasagittal section among the three age groups

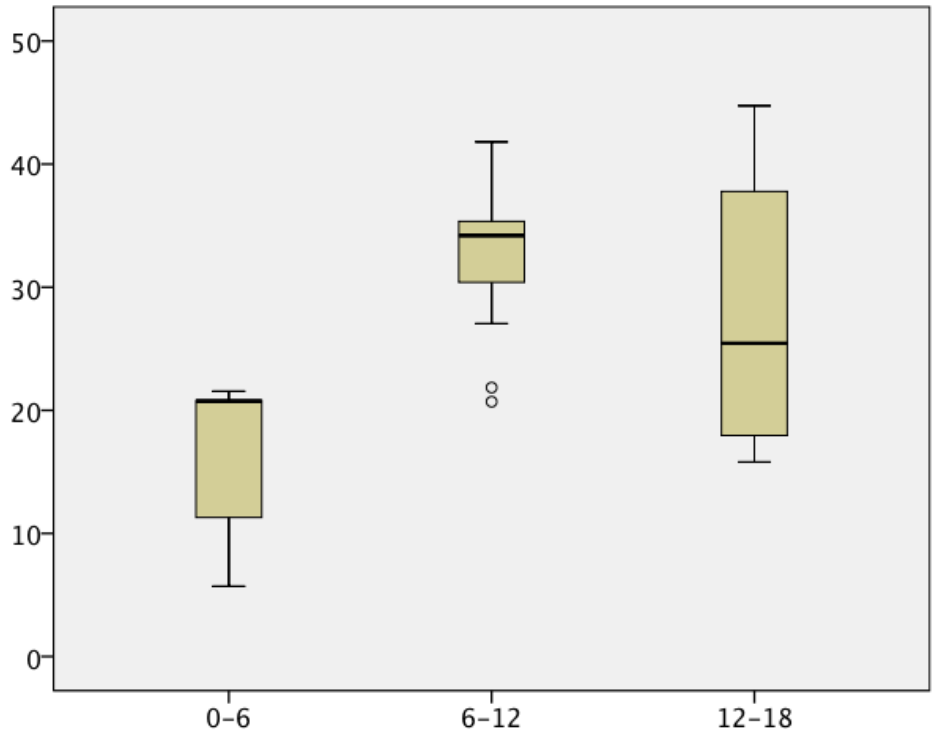

Figure 10.21. Comparison of steepness of anterior fossa slope in sagittal section among the three age groups

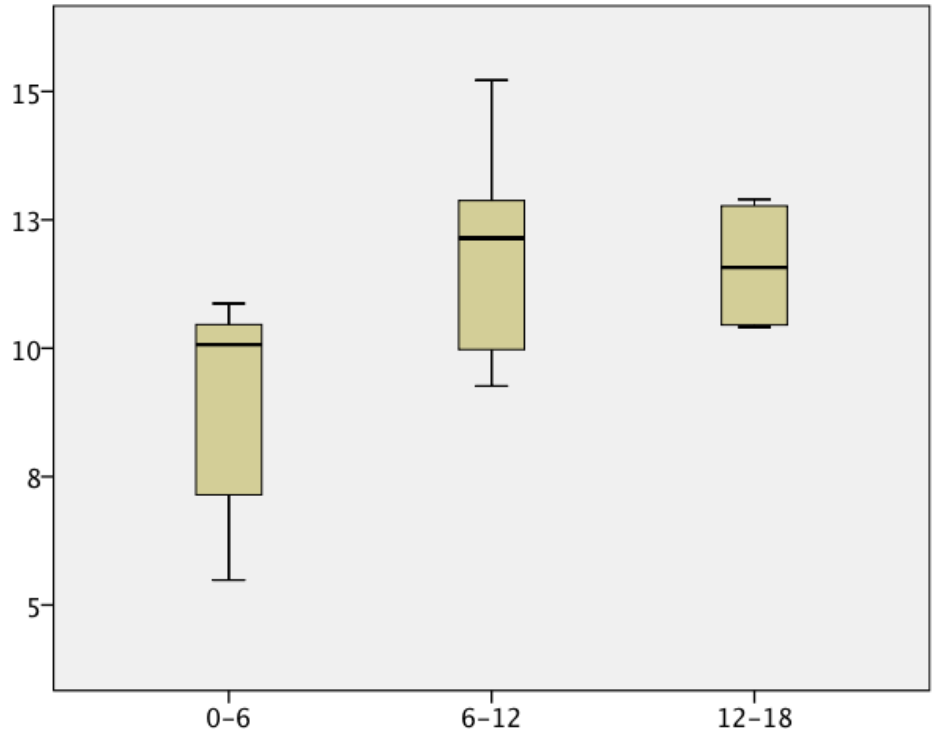

Figure 10.22. Comparison of direct length of anterior fossa slope among the three age groups

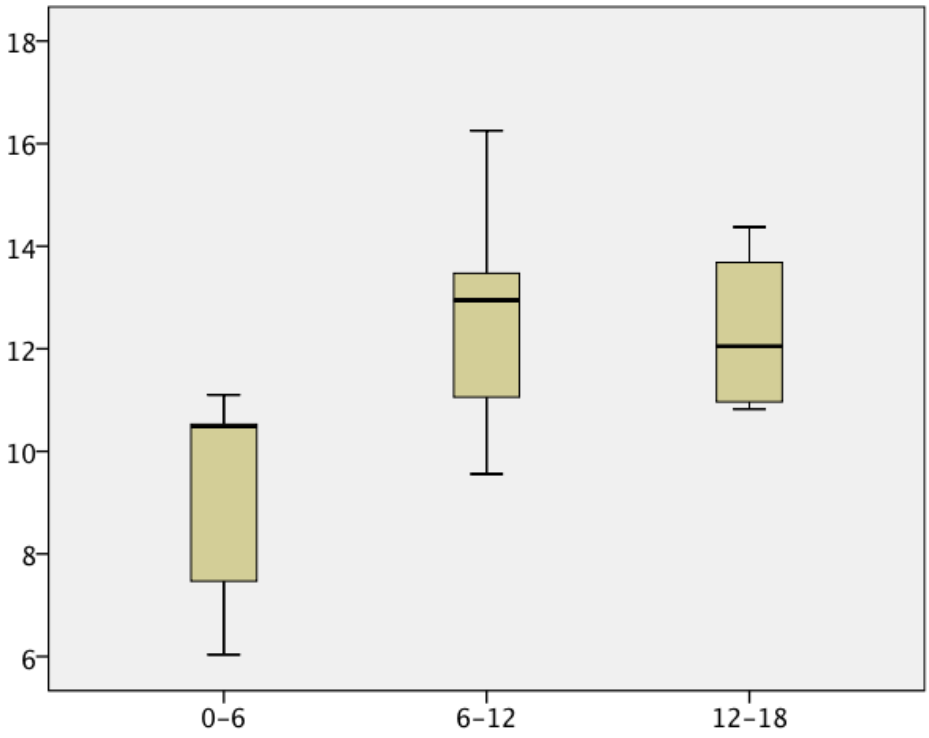

Figure 10.23. Comparison of curvilinear length of anterior fossa slope among the three age groups

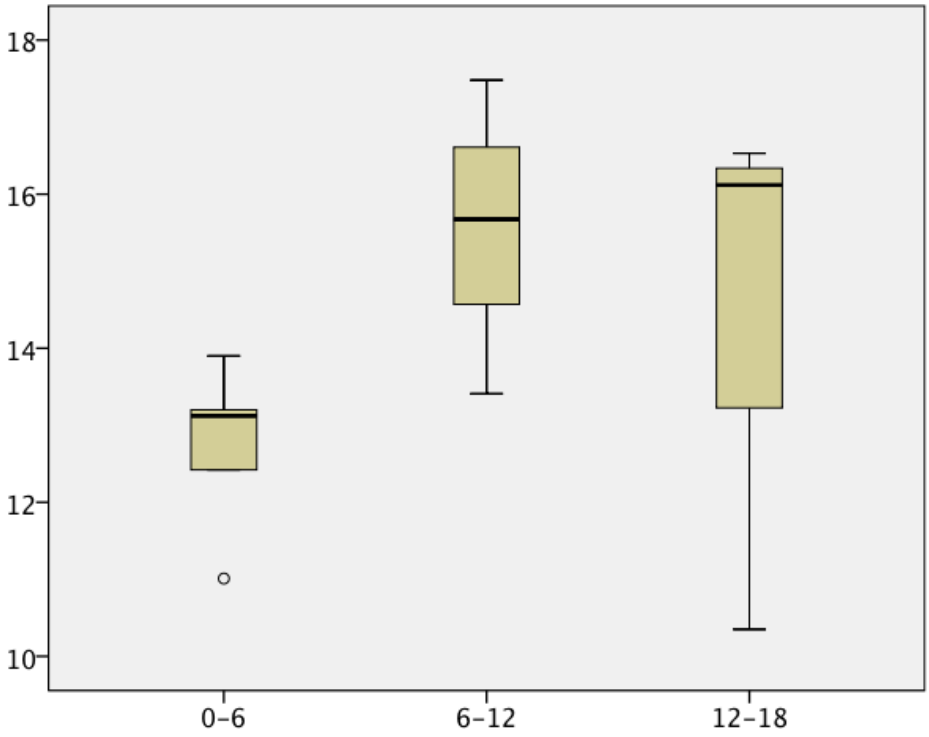

Figure 10.24. Comparison of left medio-lateral diameters among the three age groups

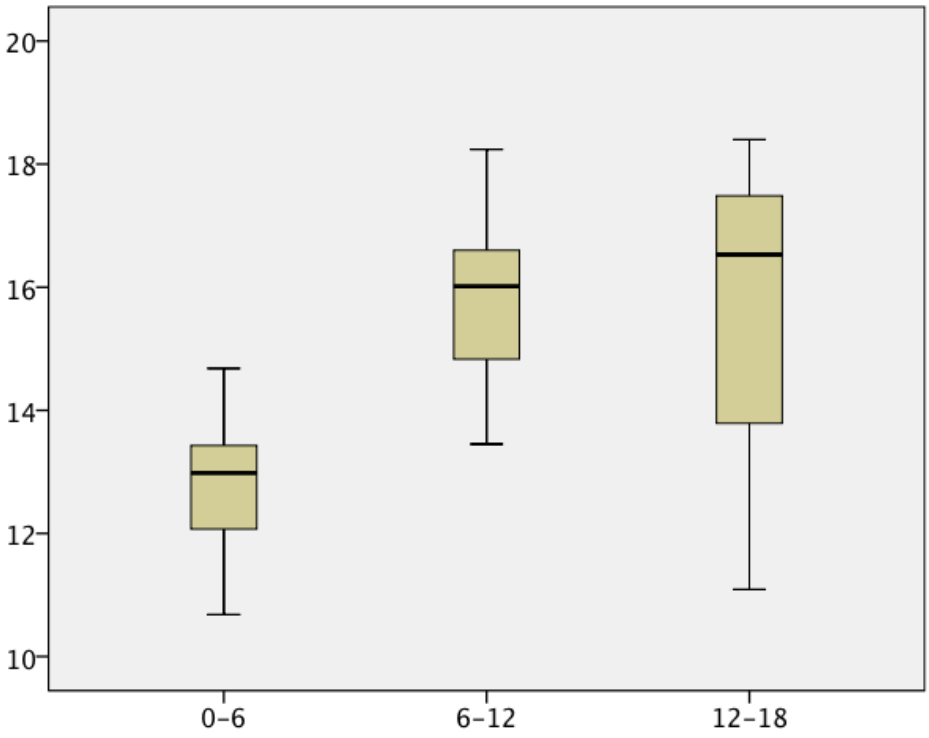

Figure 10.25. Comparison of right medio-lateral diameters among the three age groups

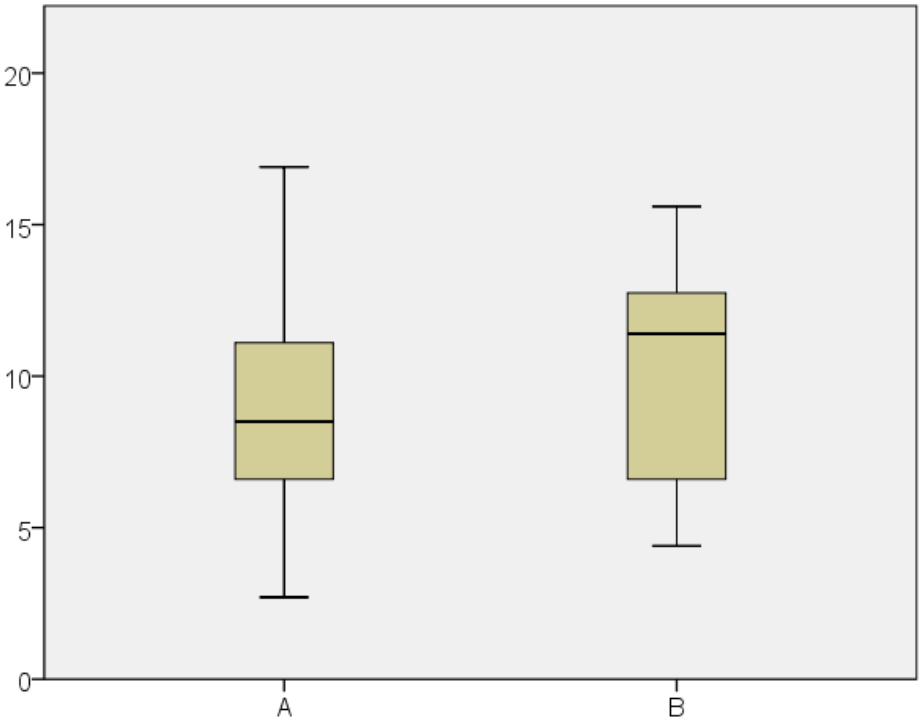

Figure 10.26. Comparison of patient's age between subjects with condyles scored as "normal/ mildly deformed" (group A) and "severely deformed" (group B)

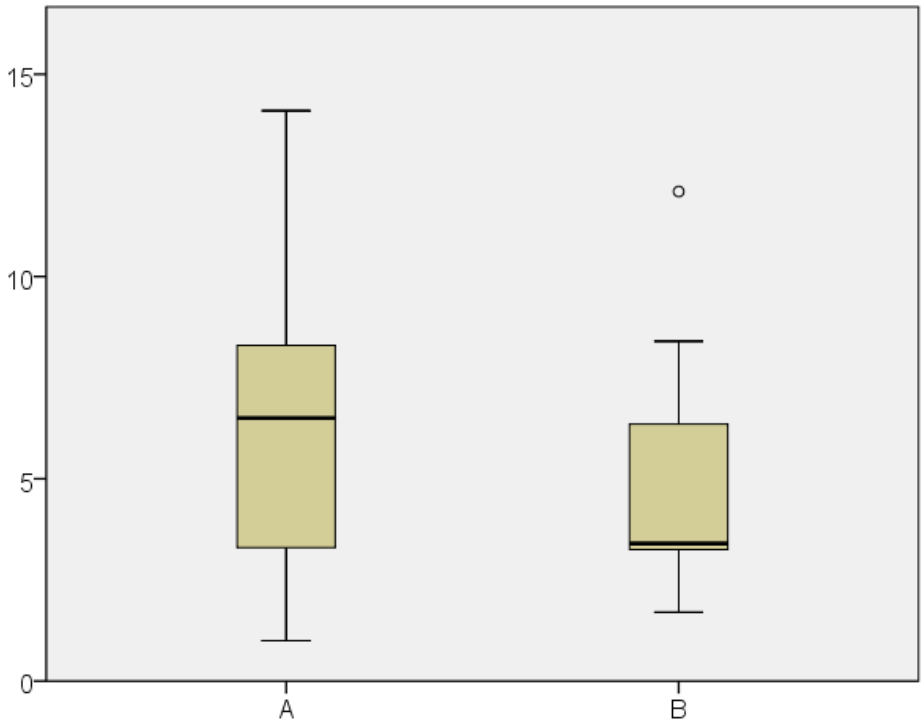

Figure 10.27. Comparison of age at diagnosis between subjects with condyles scored as "normal/ mildly deformed" (group A) and "severely deformed" (group B)

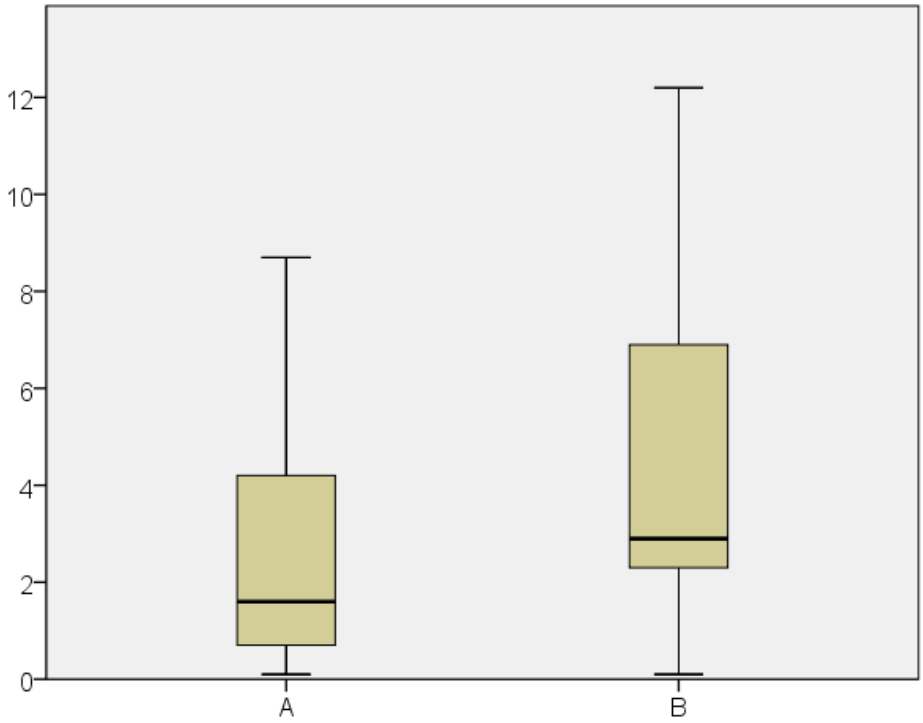

Figure 10.28. Comparison of disease duration between subjects with condyles scored as "normal/ mildly deformed" (group A) and "severely deformed" (group B)

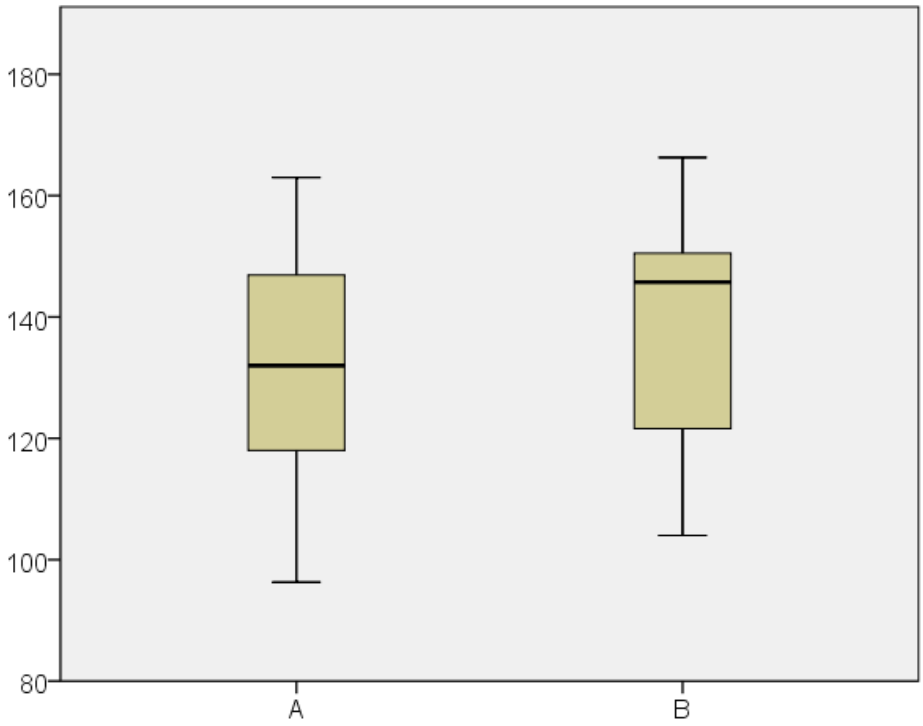

Figure 10.29. Height comparison between subjects with condyles scored as "normal/ mildly deformed" (group A) and "severely deformed" (group B)

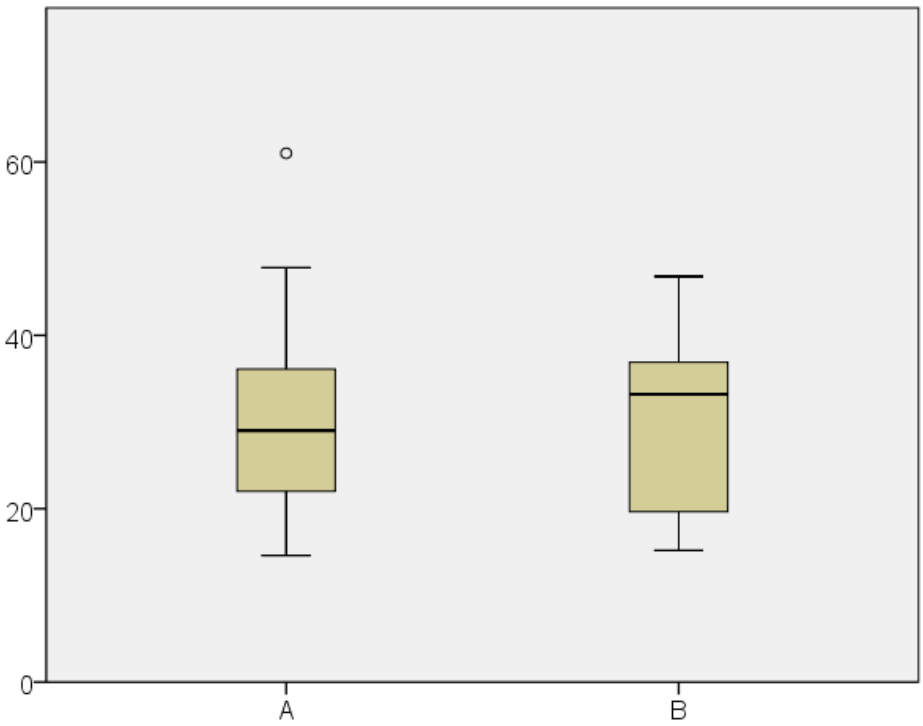

Figure 10.30. Weight comparison between subjects with condyles scored as "normal/ mildly deformed" (group A) and "severely deformed" (group B)

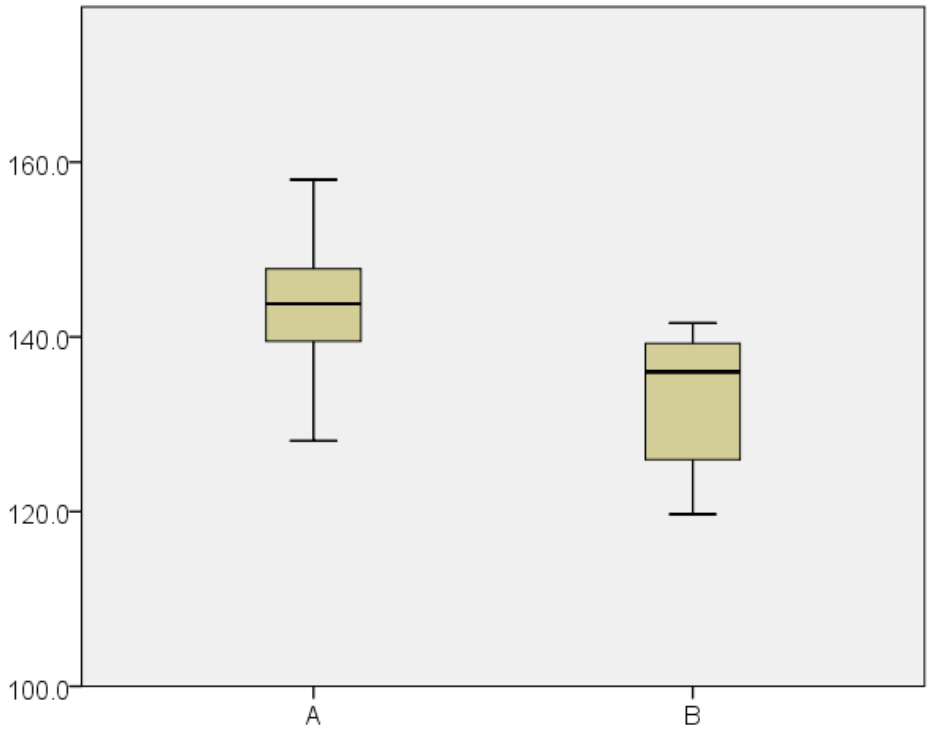

Figure 10.31. Intercondylar angle comparison between subjects with condyles scored as "normal/ mildly deformed" (group A) and "severely deformed" (group B)

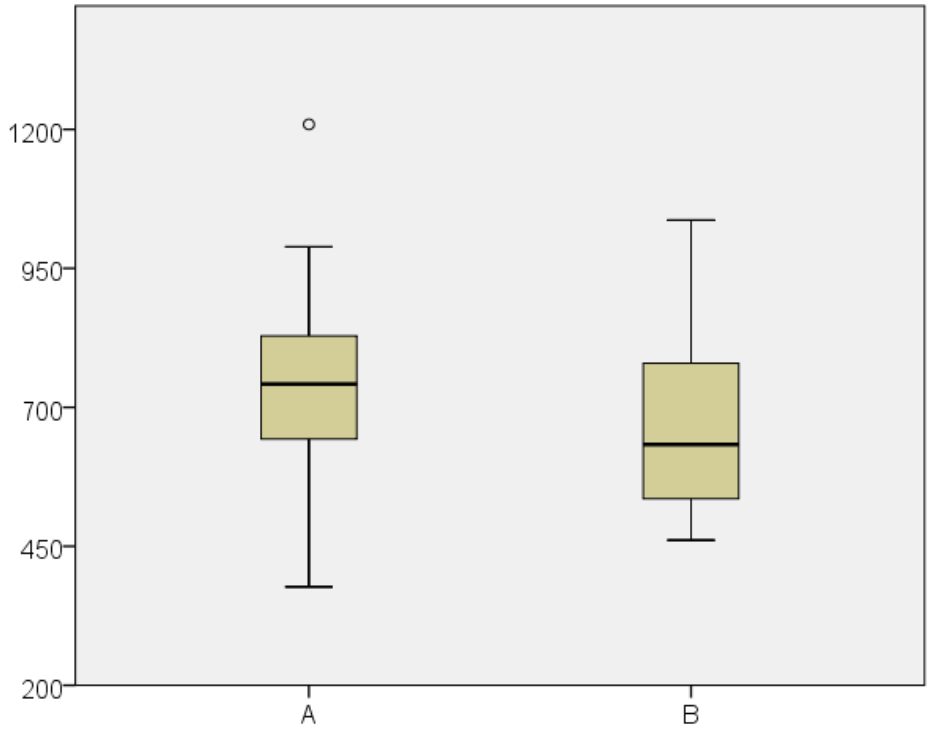

Figure 10.32. Condylar volume comparison between subjects with condyles scored as "normal/ mildly deformed" (group A) and "severely deformed" (group B)

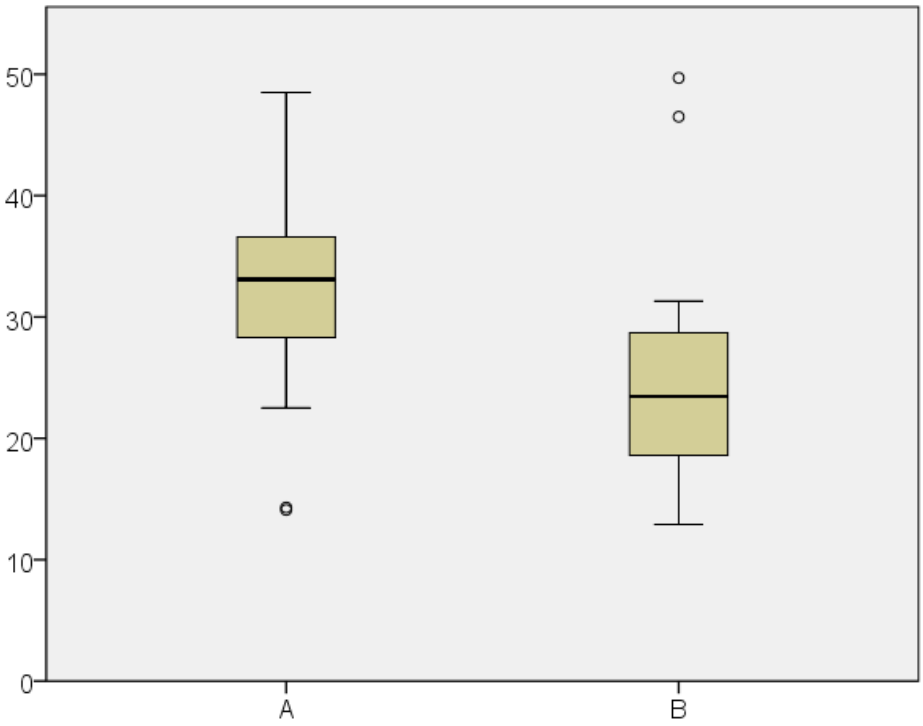

Figure 10.33. Comparison of steepness of the anterior fossa slope in parasagittal section between subjects with condyles scored as "normal/ mildly deformed" (group A) and "severely deformed" (group B)

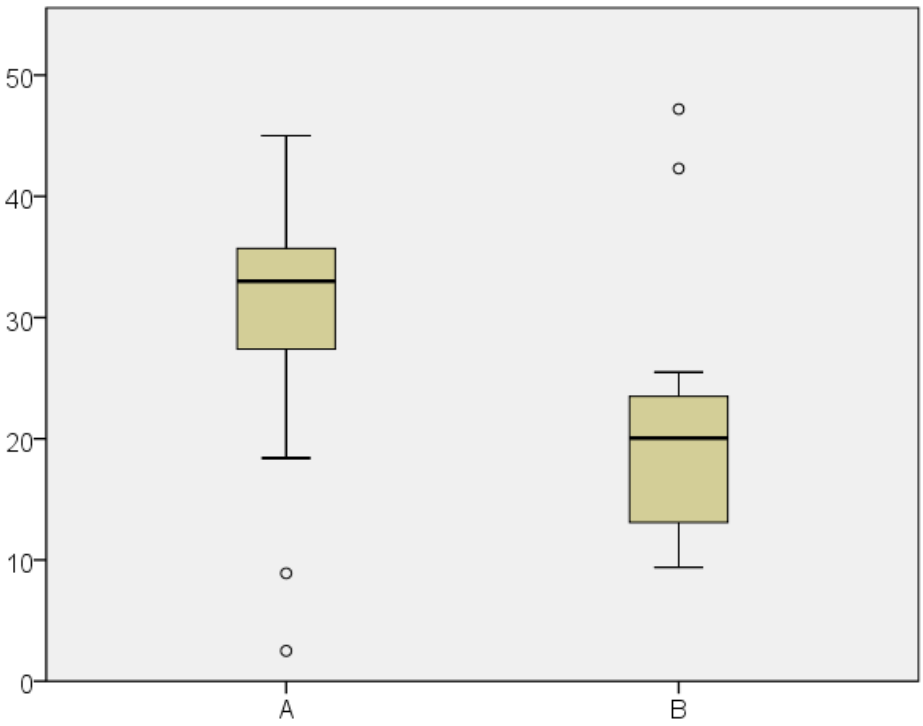

Figure 10.34. Comparison of steepness of the anterior fossa slope in sagittal section between subjects with condyles scored as "normal/ mildly deformed" (group A) and "severely deformed" (group B)

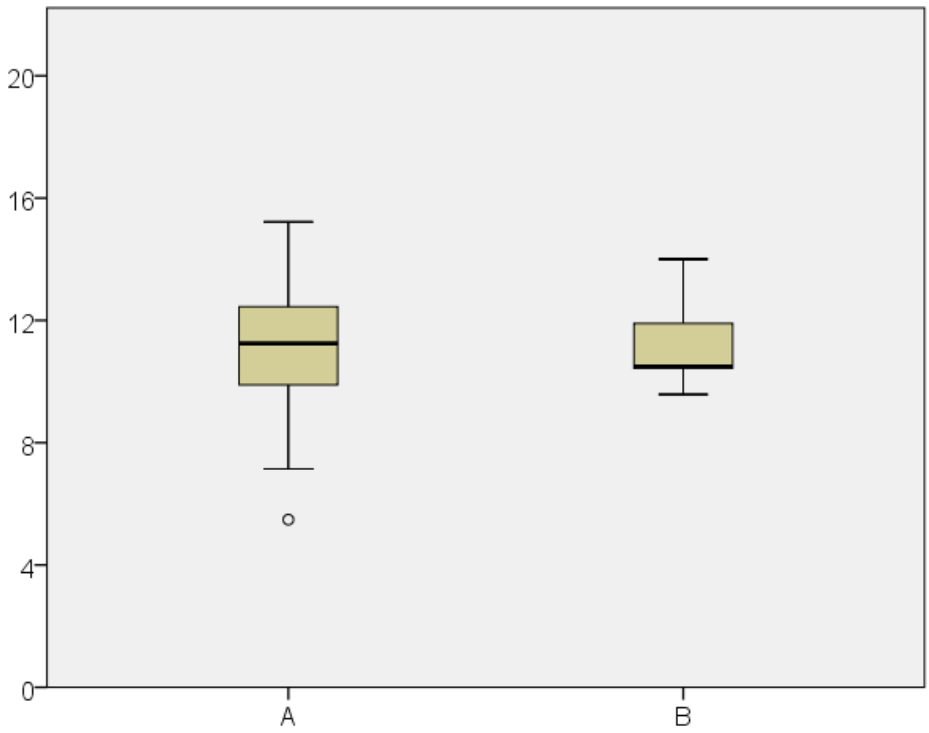

Figure 10.35. Direct length comparison between subjects with condyles scored as "normal/ mildly deformed" (group A) and "severely deformed" (group B)

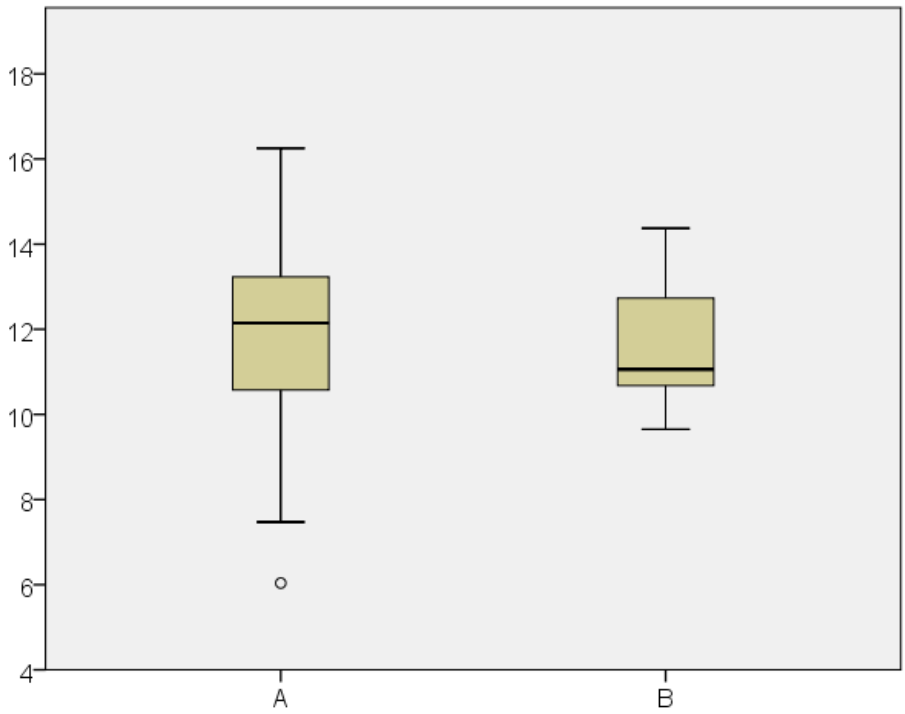

Figure 10.36. Comparison of curvilinear length between subjects with condyles scored as "normal/ mildly deformed" (group A) and "severely deformed" (group B)

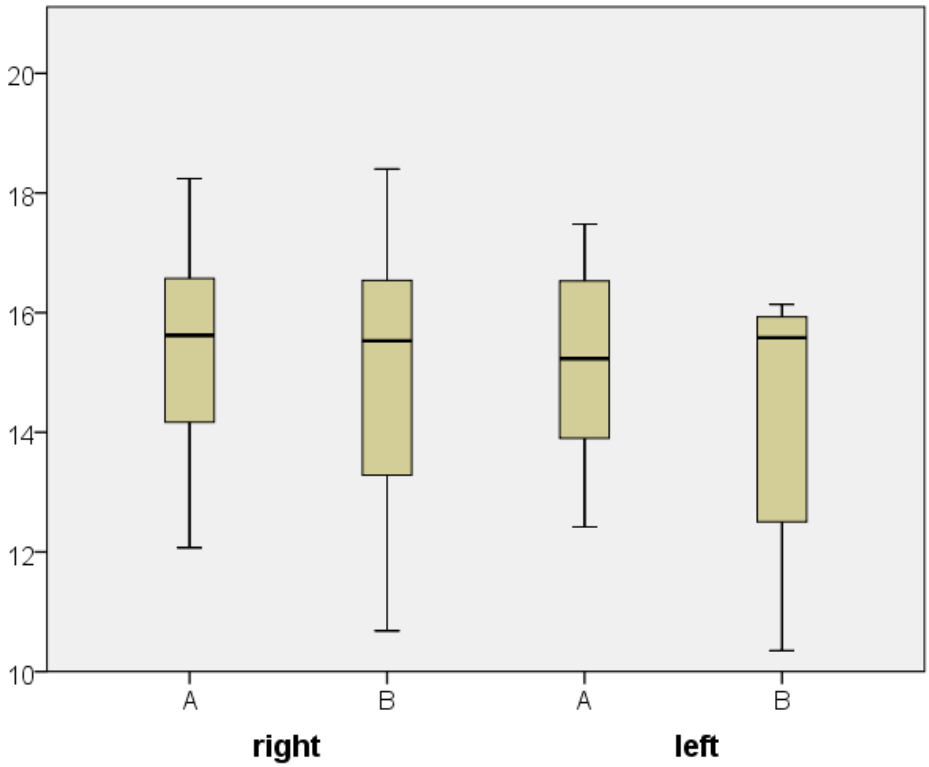

Figure 10.37. Comparison of medio-lateral diameter at the largest transversal section between subjects with condyles scored as "normal/ mildly deformed" (group A) and "severely deformed" (group B)

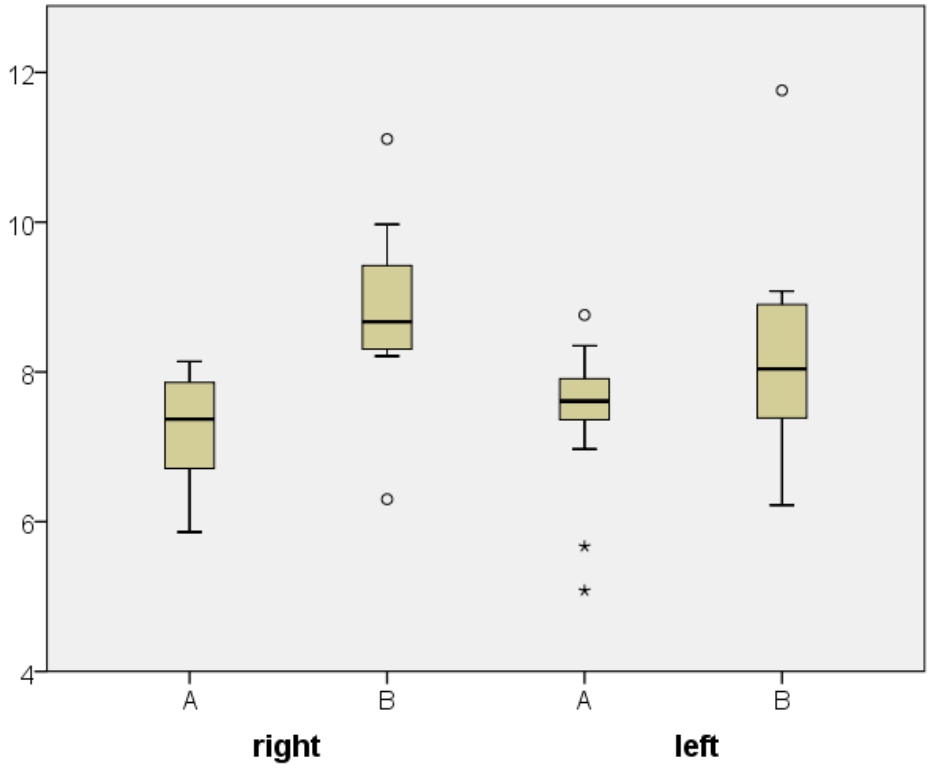

Figure 10.38. Comparison of antero-posterior diameter at the largest transversal section between subjects with condyles scored as "normal/ mildly deformed" (group A) and "severely deformed" (group B)

11 References

Cevidanes LHS, Hajati AK, Paniagua B, Lim PF, Walker DG, Palconet G, Nackley AG, Styner M, Ludlow JB, Zhu H, Phillips C. Quantification of condylar resorption in temporomandibular joint osteoarthritis. Oral Surgery, Oral Medicine, Oral Pathology, Oral Radiology, and Endodontology 2010;1:110-117

Costa ALF, Yasuda CL, Appenzeller S, Lopes SLP, Cendes F. Comparison of conventional MRI and 3D-reconstruction model for evaluation of temporomandibular joint. Surg Radiol Anat 2008;30:663–667

Ettlin DA, Mang H, Colombo V, Palla S, Gallo LM. Stereometric assessment of TMJ space variation by occlusal splints. J Dent Res 2008;87:877-881

Farronato G, Garagiola U, Carletti V, Cressoni P, Mercatali L, Farronato D. Change in condylar and mandibular morphology in juvenile idiopathic arthritis: Cone Beam volumetric imaging. Minerva Stomatol 2010;59:519-34

Gallo LM, Chiaravalloti G, Iwasaki LR, Nickel JC, Palla S. Mechanical work during stress-field translation in the human TMJ. J Dent Res 2006;85:1006-1010

Gallo LM, Nickel JC, Iwasaki LR, Palla S. Stress-field translation in the healthy human temporomandibular joint. J Dent Res 2000;79:1740-1746

Gare BA. Epidemiology of rheumatic disease in children. Curr Opin Rheumatol 1996;8:449-54

Gössi DB, Gallo LM, Bahr E, Palla S. Dynamic intraarticular space variation in clicking TMJs. J Dent Res 2004;83:480-484

Hu YS, Schneiderman ED, Harper RP. The temporomandibular joint in juvenile rheumatoid arthritis. Part II: relationship between computed tomographic and clinical findings. Pediatr Dent 1996;18:312-319

Karhulahti T, Ylijoki H, Ronning O. Mandibular condyle lesions related to age at onset and subtypes of juvenile rheumatoid arthritis in 15-year-old children. Scand J Dent Res 1993;101:332-338

Kitai N, Kreiborg S, Murakami S, Bakke M, Møller E, Darvann TA, Takada K. A three-dimensional method of visualizing the temporomandibular joint based on magnetic resonance imaging in a case of juvenile chronic arthritis. Int J Paediatr Dent 2002;12(2):109-15

Kuseler A, Pedersen TK, Herlin T, Gelineck J. Contrast enhanced magnetic resonance imaging as a method to diagnose early inflammatory changes in the temporomandibular joint in children with juvenile chronic arthritis. J Rheumatol 1998;25:1406-12

Larheim TA, Bjornland T, Smith HJ, Aspestrand F, Kolbenstvedt A. Imaging temporomandibular joint abnormalities in patients with rheumatic disease. Comparison with surgical observations. Oral Surg Oral Med Oral Pathol 1992;73:494-501

Martini G, Bacciliero U, Tregnaghi A, Montesco MC, Zulian F. Isolated temporomandibular synovitis as unique presentation of juvenile idiopathic arthritis. J Rheumatol 2001;28:1689-92

Mayne JG, Hatch GS. Arthritis of the temporomandibular joint. J Am Dent Assoc 1969;79:125-30

Müller L, Kellenberger CJ, Cannizzaro E, Ettlin D, Schraner T, Bolt IB, Peltomäki T, Saurenmann RK. Early diagnosis of temporomandibular joint involvement in juvenile idiopathic arthritis: a pilot study comparing clinical examination and ultrasound to magnetic resonance imaging. Rheumatology (Oxford) 2009;48(6):680-5

Pedersen TK, Jensen JJ, Melsen B, Herlin T. Resorption of the temporomandibular condylar bone according to subtypes of juvenile chronic arthritis. J Rheumatol 2001;28:2109-2115

Petty RE, Southwood TR, Manners P, Baum J, Glass DN, Goldenberg J, et al; International League of Associations for Rheumatology. International League of Associations for Rheumatology classification of juvenile idiopathic arthritis: second revision, Edmonton, 2001. J Rheumatol 2004;31:390-2

Ronning O, Valiaho ML, Laaksonen AL. The involvement of the temporomandibular joint in juvenile rheumatoid arthritis. Scand J Rheumatol 1974;3:89-96

Scolozzi P, Bosson G, Jaques B. Severe isolated temporomandibular joint involvement in juvenile idiopathic arthritis. J Oral Maxillofac Surg 2005;63:1368-71

Smith HJ, Larheim TA, Aspestrand F. Rheumatic and nonrheumatic disease in the temporomandibular joint: gadolinium-enhanced MR imaging. Radiology 1992;185:229-34

Still GF. On a form of chronic joint disease in children. Medico-chirurgical Transactions 1897;80:47-59

Twilt M, Mobers SM, Arends LR, et al. Temporomandibular involvement in juvenile idiopathic arthritis. J Rheumatol 2004;31:1418-1422

12 Acknowledgements

I would like to thank

- Prof. Dr. sc. techn. L.M. Gallo for providing this interesting and challenging topic and supervising me during the whole time
- PD Dr. med. et med. dent. D. Ettlin for always having time for me and giving valuable and encouraging inputs
- Dr. med. dent. L. Müller and Dr. med. C. Kellenberger for providing the data and sharing their reflections on my work
- Mr. S. Erni for technical support
- last but not least, my family and friends for continuing mental and moral support.

13 Appendix A

In the following, right and left condyles of all subjects are graphically presented, sorted by age, with subtype of JIA listed in brackets:

1st row: frontal (left), axial (middle) and sagittal (right) views.

2nd row: transparent axial view of fossa-condyle relationship.

	right	left
# 25; age 2.7 (oligoarthritis)	*no deformation*	*no deformation*
		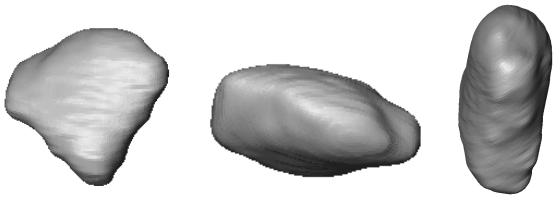
	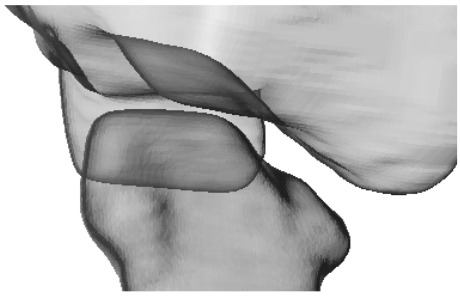	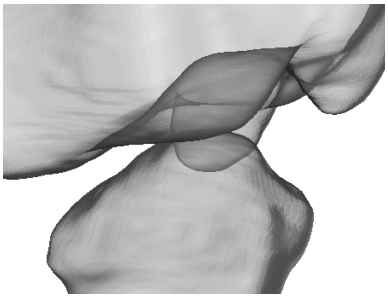
# 12; age 3.8 (oligoarthritis)	*no deformation*	*no deformation*
	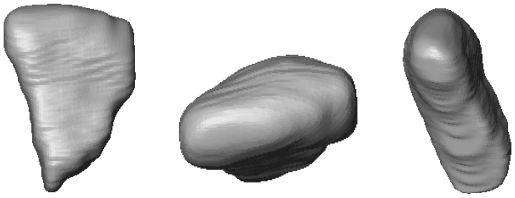	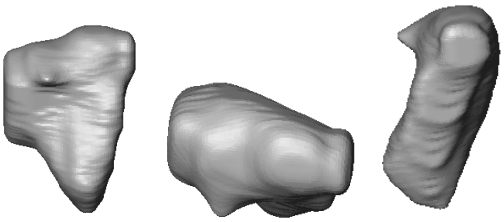
	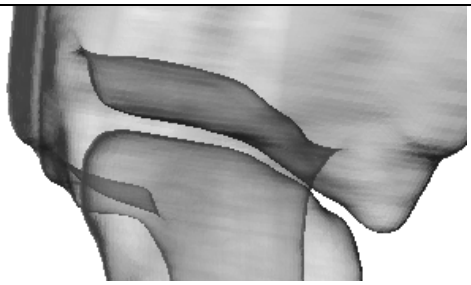	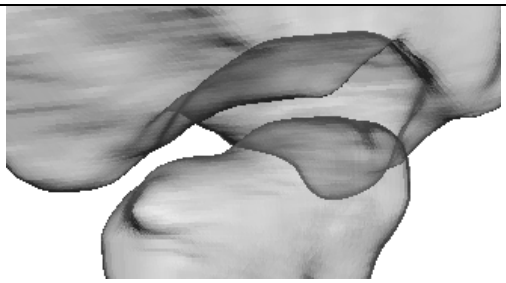

# 18; age 4.4 (ext. oligoarthritis)	*severe deformation*	*severe deformation*
	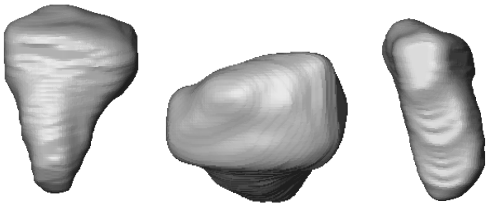	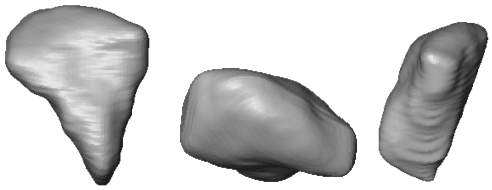
	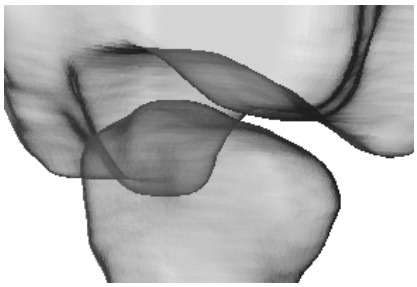	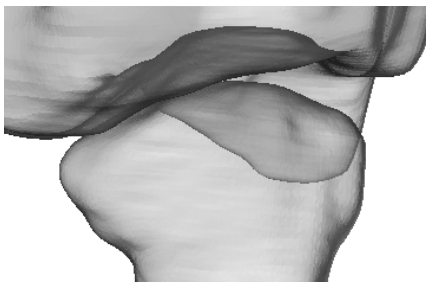
# 5; age 4.7 (oligoarthritis)	*no deformation*	*no deformation*
	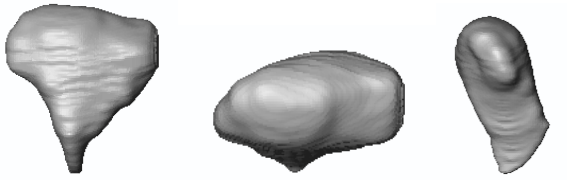	
	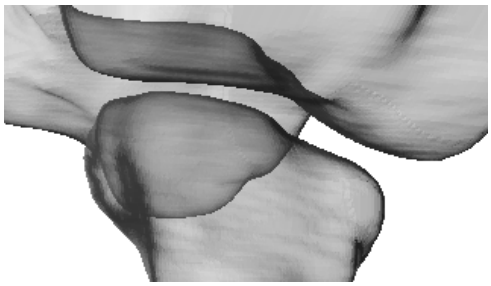	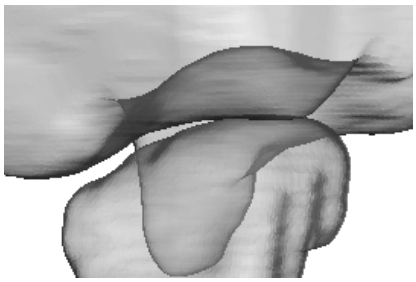
# 26; age 4.8 (polyarthritis)	*no deformation*	*no deformation*
	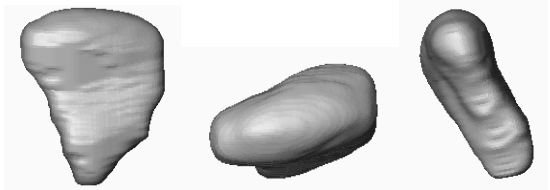	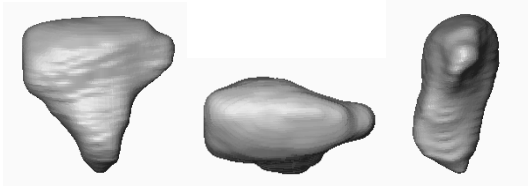
	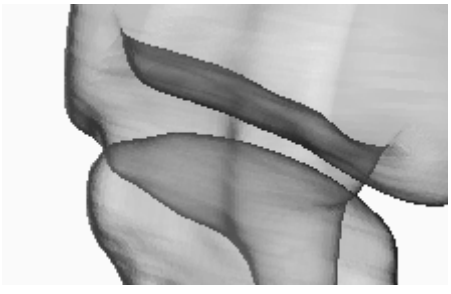	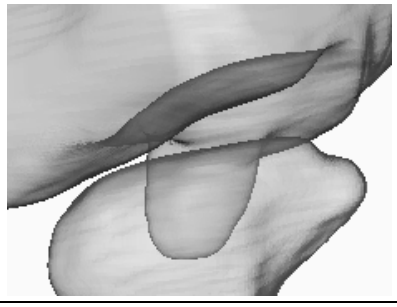

# 21; age 5.3 (polyarthritis)	*no deformation*	*severe deformation*
	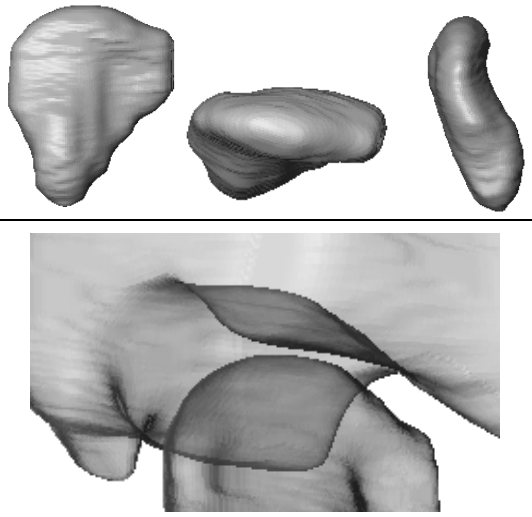	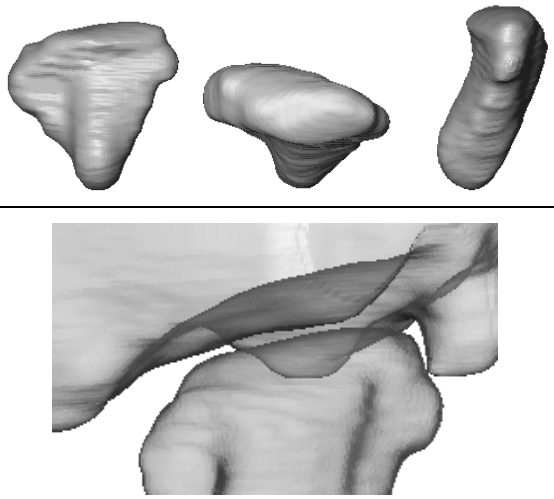
# 10; age 6.2 (polyarthritis)	*no deformation*	*no deformation*
	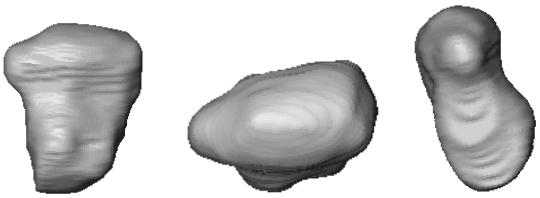	
	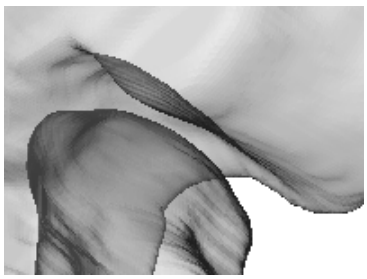	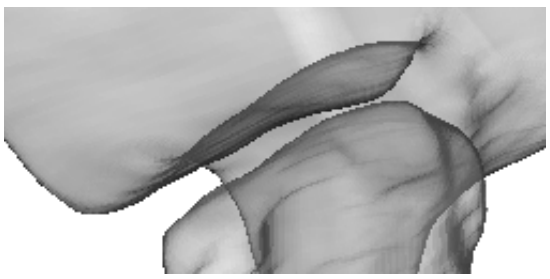
# 4; age 6.6 (oligoarthritis)	*no deformation*	*no deformation*
	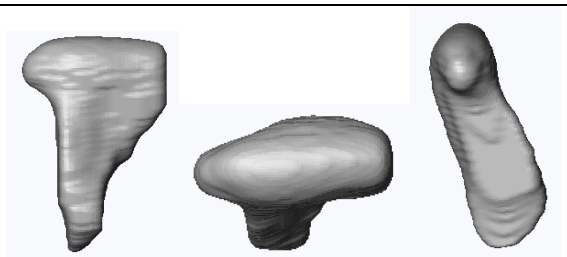	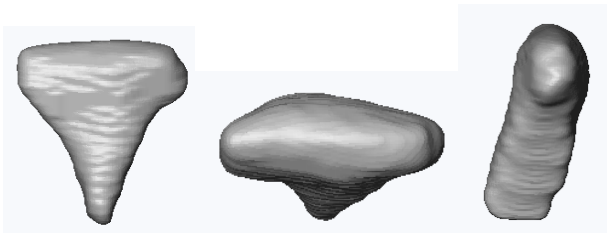
	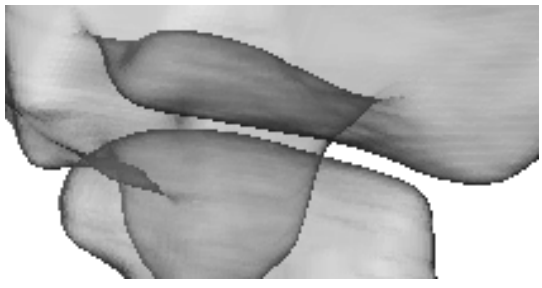	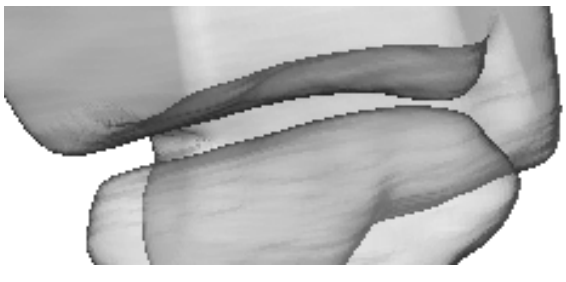

# 15; age 6.9 (oligoarthritis)	*no deformation*	*no deformation*
	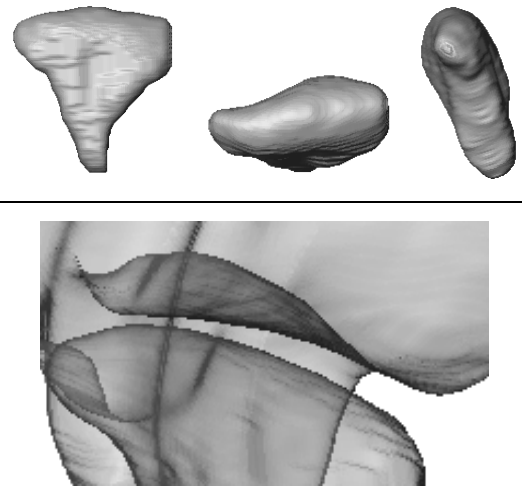	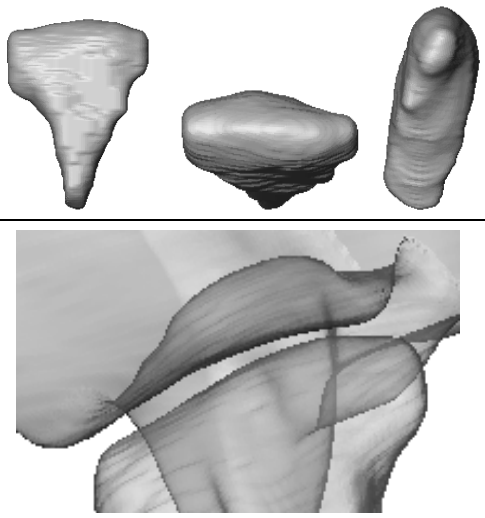
# 20; age 7.7 (oligoarthritis)	*mild deformation*	*no deformation*
	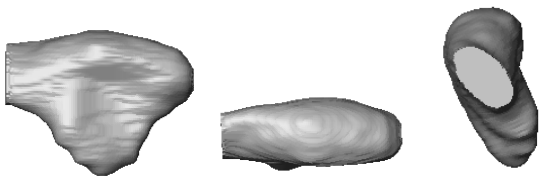	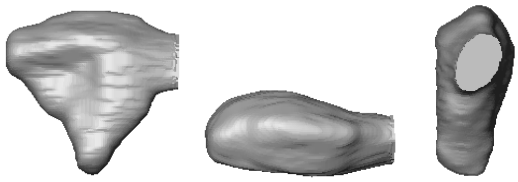
	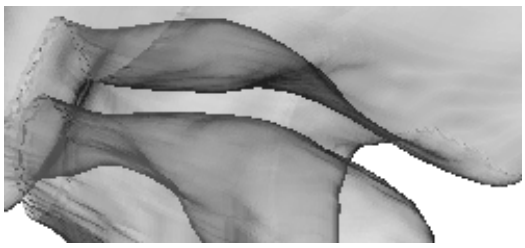	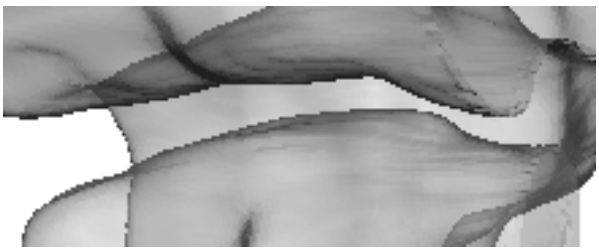
# 8; age 7.9 (polyarthritis)	*severe deformation*	*severe deformation*
	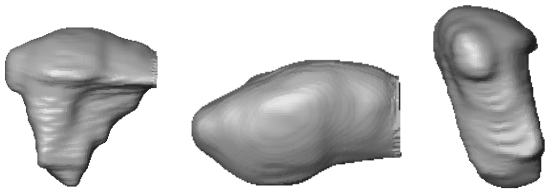	
	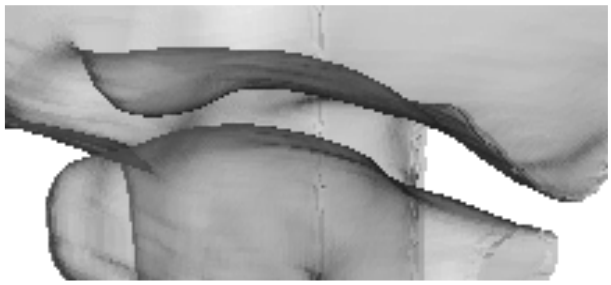	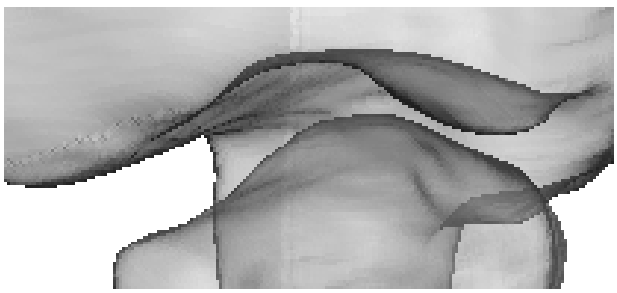

# 3; age 7.9 (psoriatic arthritis)	*no deformation*	*no deformation*
	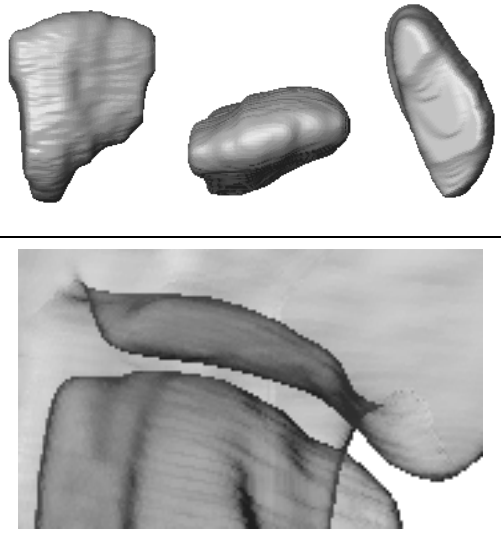	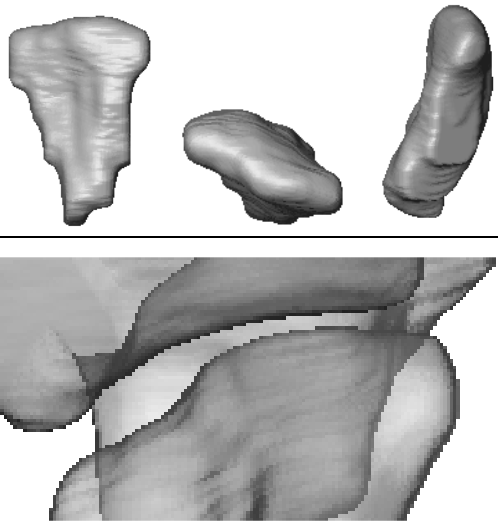
# 11; age 8.3 (polyarthritis)	*no deformation*	*no deformation*
	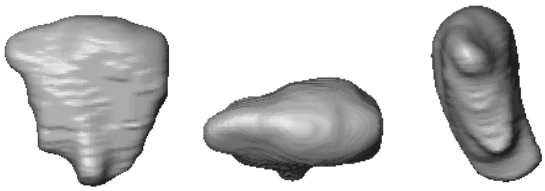	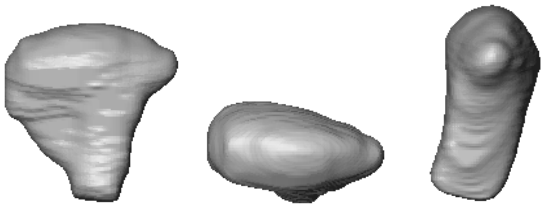
	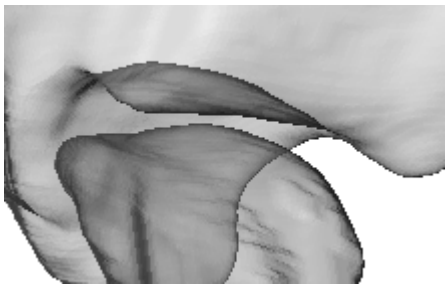	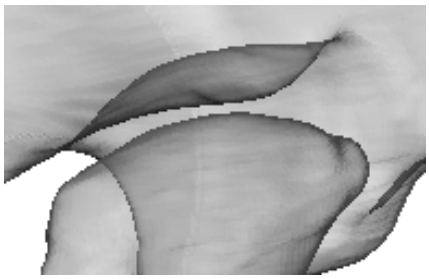
# 2; age 8.5 (polyarthritis)	*mild deformation*	*mild deformation*
	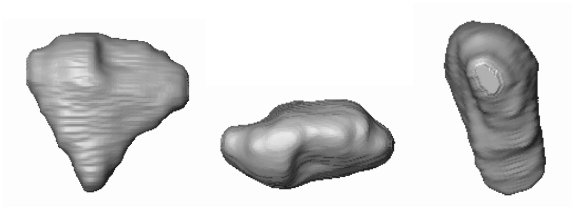	
	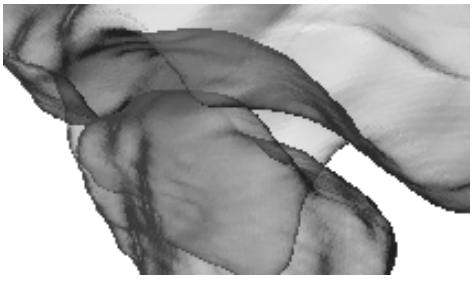	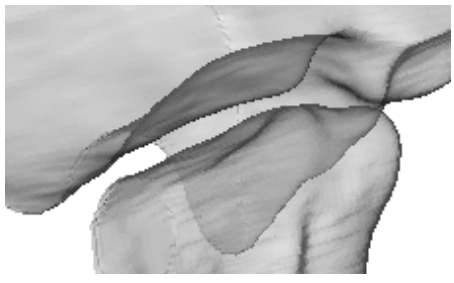

# 7; age 9.7 (polyarthritis)	*no deformation*	*no deformation*
	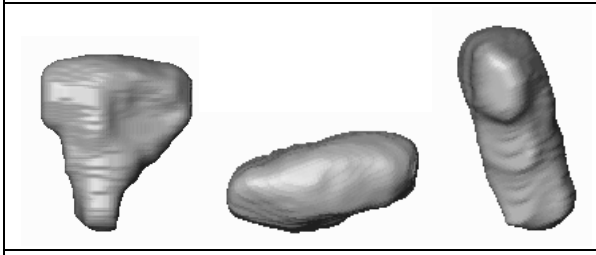	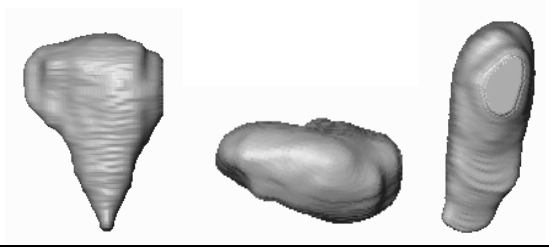
	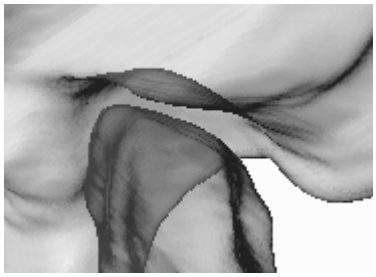	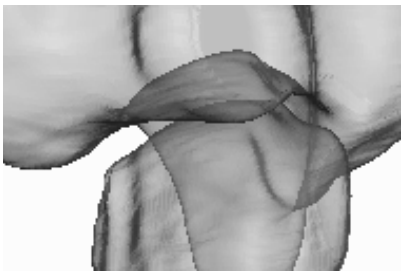
# 24; age 10.4 (ER-arthritis)	*no deformation*	*no deformation*
	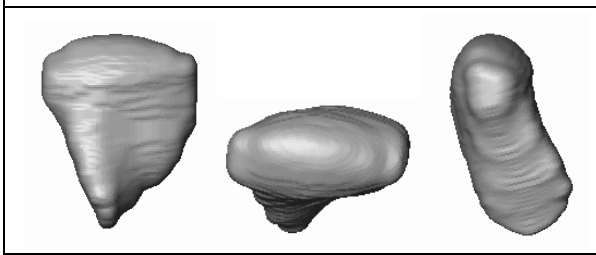	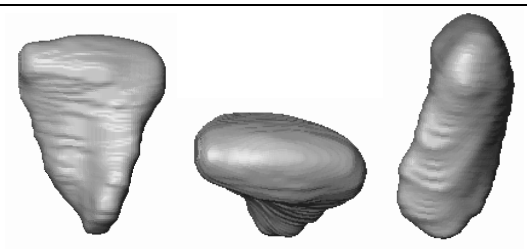
	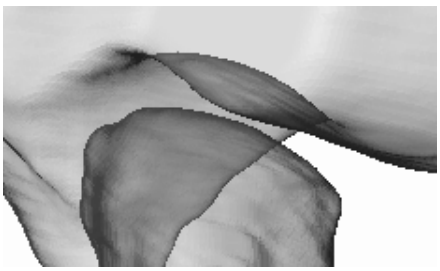	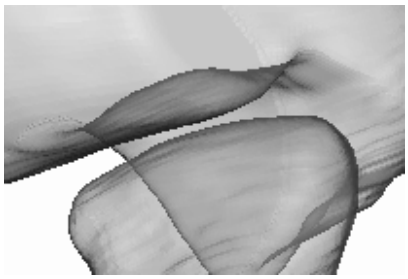
# 17; age 10.5 (oligoarthritis)	*no deformation*	*no deformation*
	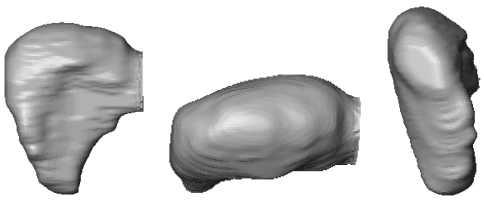	
	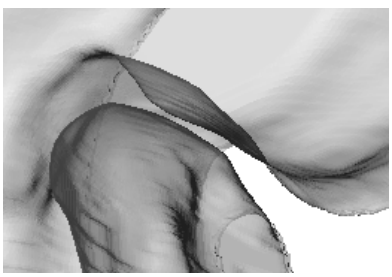	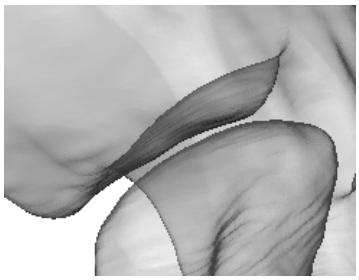

# 27; age 10.7 (ER-arthritis)	*no deformation*	*no deformation*
		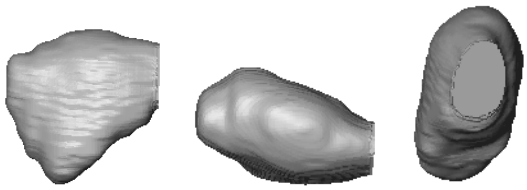
	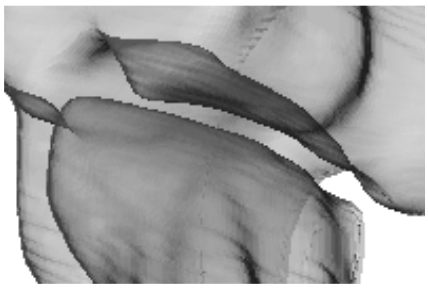	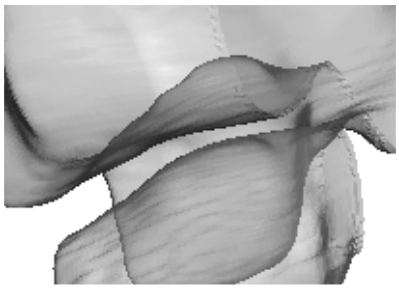
# 1; age 11.1 (oligoarthritis)	*no deformation*	*no deformation*
	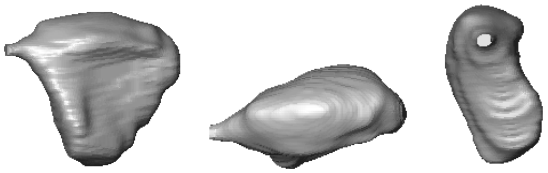	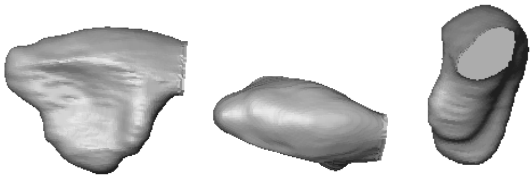
	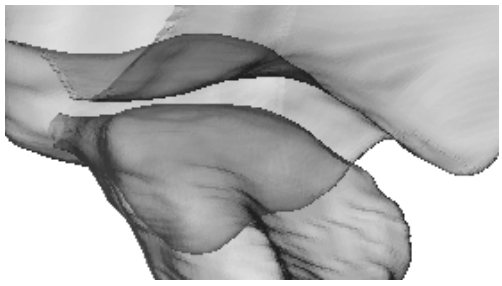	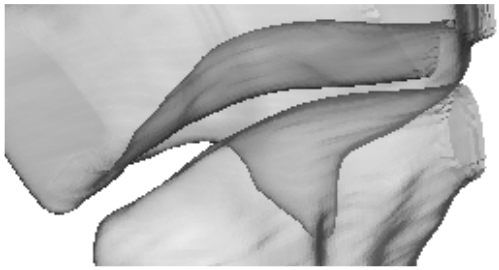
# 28; age 11.4 (oligoarthritis)	*severe deformation*	*severe deformation*
	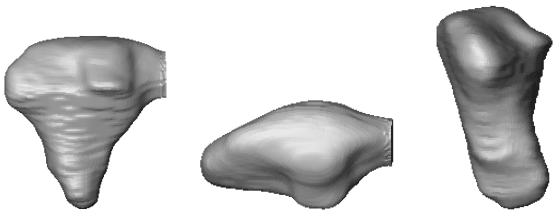	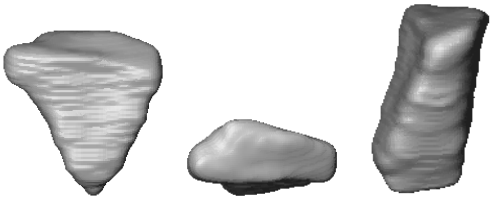
	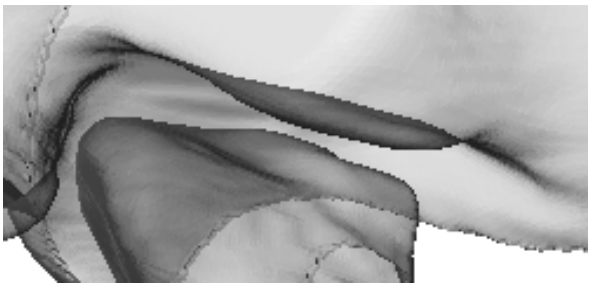	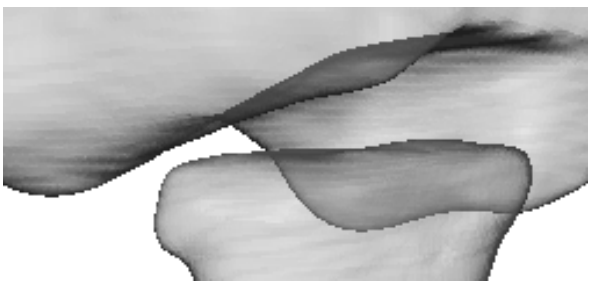

# 13; age 11.5 (oligoarthritis)	*no deformation*	*no deformation*
	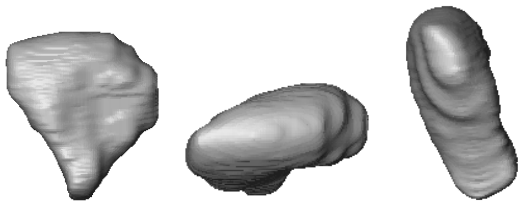	
	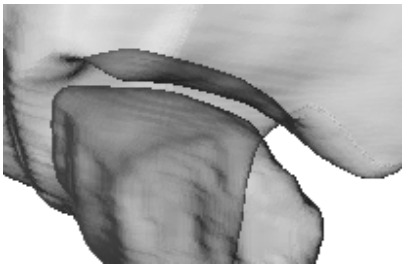	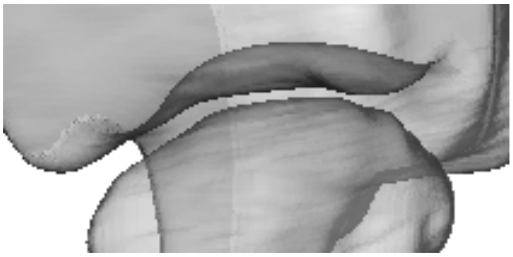
# 22; age 11.6 (ext. oligoarthritis)	*no deformation*	*no deformation*
	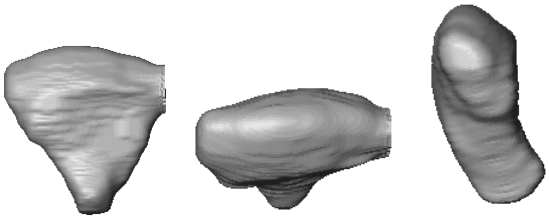	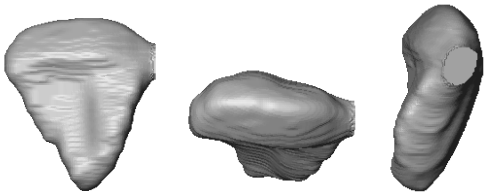
	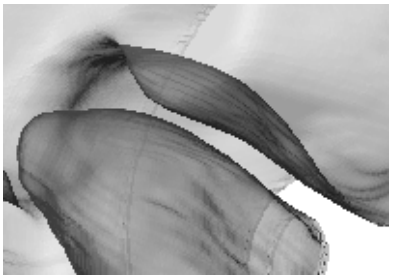	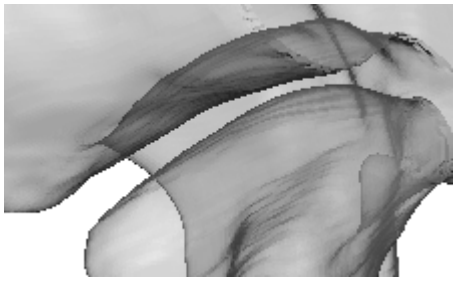
# 14; age 11.8 (ER-arthritis)	*no deformation*	*no deformation*
	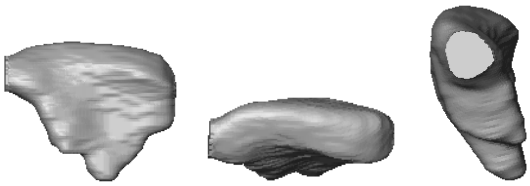	
	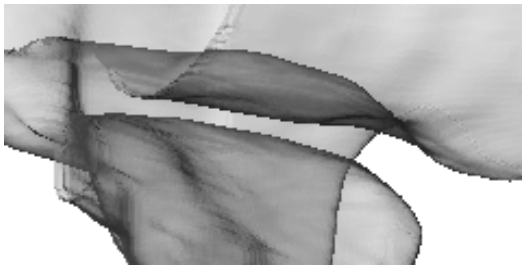	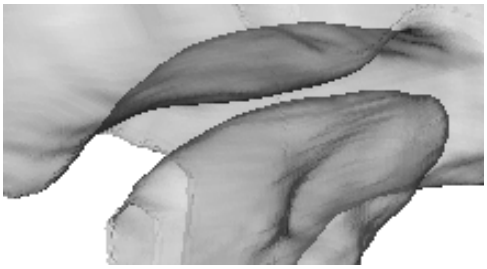

# 16; age 11.8 (polyarthritis)	*no deformation*	*no deformation*
	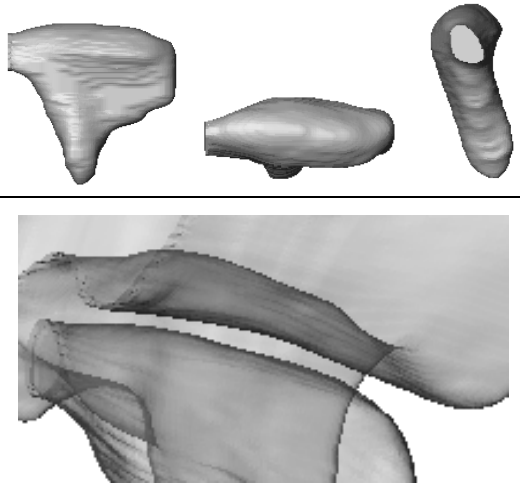	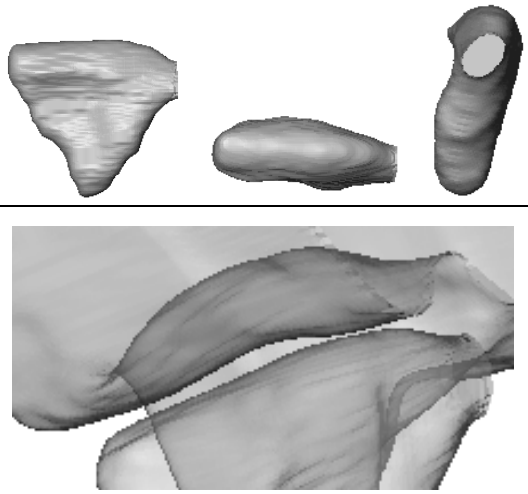
# 6; age 12.2 (polyarthritis)	*severe deformation*	*severe deformation*
	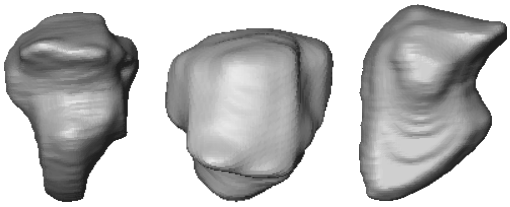	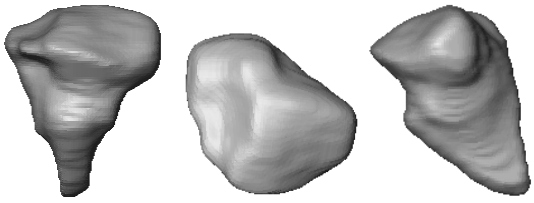
	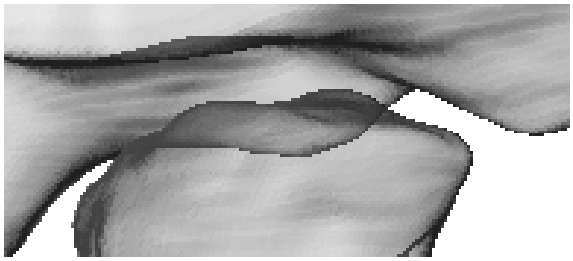	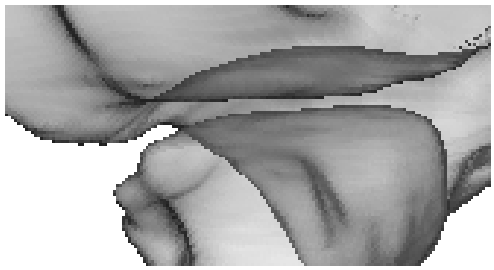
# 9; age 13.3 (ext. oligoarthritis)	*severe deformation*	*severe deformation*
	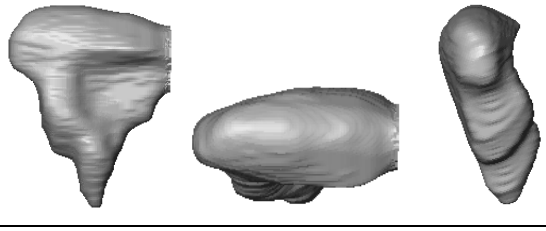	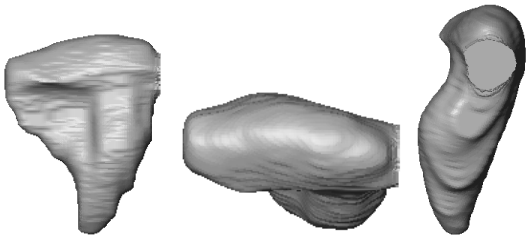
	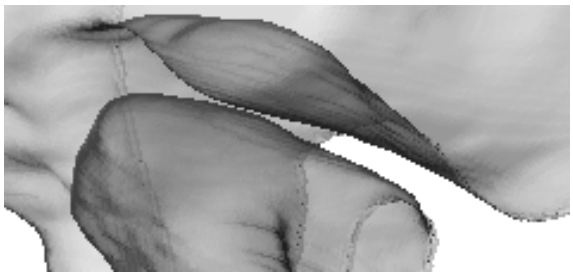	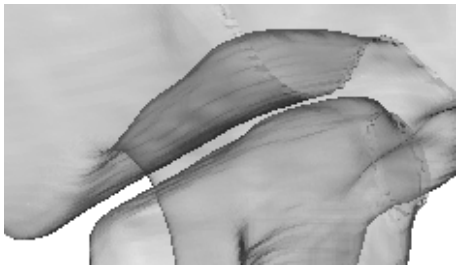

# 23; age 15.6 (polyarthritis)	*no deformation*	*severe deformation*
	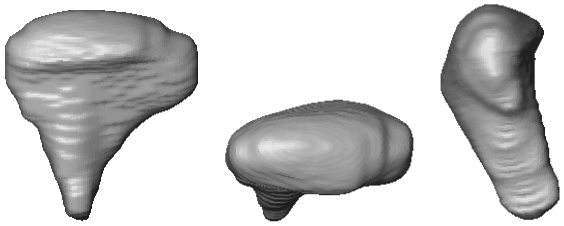	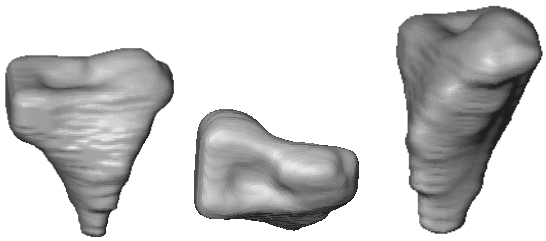
	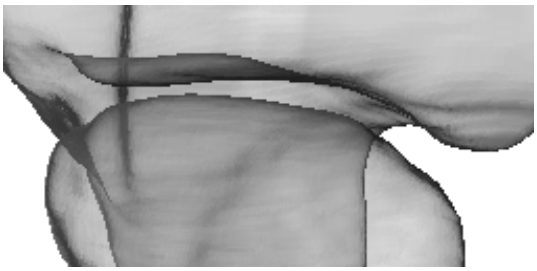	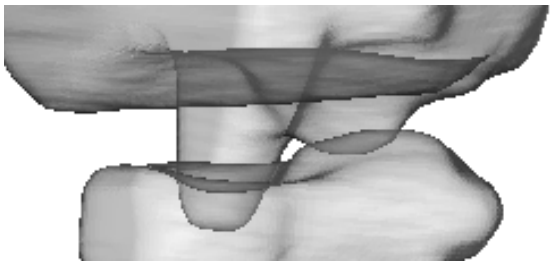
# 19; age 16.9 (polyarthritis)	*no deformation*	*no deformation*